PSR Report 2628

NoiseProp: A Dynamic 60 kHz to 30 MHz Atmospheric Radio Noise Model

Ronald M. Bloom
David M. Crandall
Chris R. Warber

March 1996

Final Report
Contract N00014-94-C-0053

Prepared for

Office of Naval Research
Ballston Tower One
800 North Quincy Street
Arlington, VA 22217-5660

PACIFIC-SIERRA RESEARCH CORPORATION
2901 28th Street • Santa Monica, CA 90405 • (310) 314-2300, FAX (310) 314-2323

NONPRINT FORM

1. Type of Product:	2.Operating System/Version:	3. New Product or Replacement:	4. Type of File:
Computer Disk	Windows95	New	Database

5. Language/Utility Program:

n/a

WORKING COPY

6. # of Files/#of Products	7. Character Set:	8. Disk Capacity
2 disks/ 3 files	Binary	1.4MB
	9. Compatability:	**10. Disk Size:**
	PC	3 1/2"

11. Title:

NOISEPROP: LF, MF, and HF Noise Progation Prediction

12. Performing Organization:	13. Performing Report #:	14. Contract #:
PacificSierra Research Corp. Santa Monica, CA 90405	PSR Report 2628	N)))14-94-C-0053
		15. Program Element #: n/a

16. Sponsor/Monitor:	17. Sponsor/Monitor Acronym:	19. Project #: n/a
Office of Naval Research One Ballston Tower One 800 North Quincy St. Arlington, VA 22217-5660	n/a	**20. Task #:** n/a
	18. Sponsor/Monitor #: n/a	**21. Work Unit #:** n/a

22. Date:	23. Classification of Product:
March 1996	Unclassified
24. Security Classification Authority	**25. Declassification/Downgrade Schedule**

26. Distribution/Availability A: Approved for public release; Distribution unlimited

27. Abstract:

The combined progation and lightning source algorithm are contained in a Windows-95 based graphical user interface shell called NoiseProp. This program uses as data either the original satellite-based GLO maps or the dynamic, meteorologically based DGLO maps as they become available.

28. Classification of Abstract:	**29. Limitation of Abstract:**
Unclassified	Unlimited

30. Subject Terms:

31. Required Peripherals:

32. # of Physical Records:	**33. # of Logical Records:**	**34. # of Tracks:**
35. Record Type:	**36. Color:**	**37. Recording System:**
38. Recording Density:	**39. Parity:**	**40. Playtime:**

41. Playback Speed:	**42. Video**	**43. Text:**	**44. Still Photos:**	**45. Audio:**

46. Other: NOISPROP requires WINDOWS95 and 5 MB of hard disk space.

47. Documentation/Supplemental Information:

Also includes hardcopy report: NoiseProp: A Dynamic 60 Khz to 30 Mhz Atmospheric Radio Noise Model

48. Point of contact/Telephone #:

Office of Naval Research: 703-696-6993

PREFACE

This report describes a broadband (60 kHz to 30 MHz) electromagnetic background noise model (NoiseProp). The model is conceptually similar to the PSR longwave noise model LNP, released in 1991. Global distributions of lightning activity divided into seasonal and diurnal maps are used to determine a set of elemental noise transmitters. The power radiated by each transmitter is proportional to the lightning flash rate at that location and to an empirically determined energy spectrum (which varies roughly as f^{-2}). The radiated power is then propagated by a variety of propagation algorithms (LF, MF, HF) to the receiver. The overall noise power at the receiver is taken to be an incoherent sum of power propagated from each significant noise transmitter.

The report additionally describes methods developed which will allow certain up-to-date and forecasted weather data to be converted to lightning activity (flash rate) maps. In this way, the NoiseProp model can be made to predict atmospheric noise dynamically rather than simply long term median values.

A Windows-95 based graphical user interface for the NoiseProp has been developed and is described in the Appendix.

TABLE OF CONTENTS

FIGURES

FIGURES (Continued)

1.0 INTRODUCTION

In 1991 Pacific-Sierra Research (PSR) Corporation completed a PC-based long wave noise prediction model (LNP) [Warber and Field, 1991]. LNP calculates worldwide median narrow band noise power in the ELF (50 to 300 Hz) and VLF (10 to 60 kHz) bands by summing radiated power from worldwide distributions of lightning flashes. The lightning flash data are contained in seasonal and diurnal global lighting occurrence (GLO) maps synthesized from two years of the Japanese ECS-b satellite (1978 to 1980) HF sensor lightning observations. LNP was designed as a physics based alternative to the standard CCIR empirical global noise radio model [CCIR, 1988], comparable to but more sophisticated than the WGL noise model [Maxwell et al., 1970].

The work described in this report consists of extensions to the predictive methodology of LNP applied to the joint problem of 1) LF, MF, HF radio noise prediction (60 kHz to 30 MHz) and 2) development of a capability to supplement the original long-term historical GLO maps with short-term dynamic global occurrence data (DGLO) based on certain relevant meteorological data.

- Work detailing the correlation between lightning flash rate and certain commonly available meteorological parameters (and plans for the association of such data into the LNP noise prediction system) was done under DNA sponsorship and is described completely in PSR Report 2605 [Warber and Sinclair, 1995]. By augmenting the physical basis of the noise model in this manner it will be possible to predict radio noise for short or near real time meteorological conditions. The existing, widely used models (e.g., CCIR) rely strictly on long-term averages and cannot adjust to specific weather (hence, lightning flash rate) conditions.
- The existing LNP algorithms propagated ELF/VLF RF energy in an earth-ionospheric waveguide quasi-exponential mode sum along each great circle path from lightning source region to receiver. [Actually all lightning activity in a $10^\circ \times 10^\circ$ cell is referenced to an equivalent noise transmitter (ENT) at the center of mass of the cell.] The waveguide mode formulation [Budden, 1966] is impractical for frequencies above ~100 kHz, as large numbers of discrete modes must be summed. The search for discrete modes at higher frequencies also is hampered by the tendency of the modal parameters (propagation constants) to coalesce as the wave frequency is raised. Our propagation algorithms will therefore be different from LNPs. They are a combination of ray-methods with some diffractive corrections and purely

empirical methods used in the transitional upper MF lower HF band where the closeness of the gyro-frequency is a crucial determinant of propagation.

- Additionally, the original lightning stroke spectra used in LNP have been extended above 60 kHz using the available empirical data.

2.0 NOISEPROP PROGRAM

The combined propagation and lightning source algorithm are contained in a Windows-95 based graphical user interface shell called NoiseProp. The NoiseProp program uses as data either the original satellite-based GLO maps or the dynamic, meteorologically based DGLO maps as they become available. NoiseProp allows the user to select one or several locations using an interactive map. Subsequently, radio noise in a given bandwidth as a function of local time at a fixed frequency (or ate several frequencies at a fixed time) is computed and displayed. The noise level is normally the median (50^{th} percentile). Noise exceeded an arbitrary (0.0001 to 99.999) percentage of time can also be computed. The noise is in units of dB relative to kTb where k is Boltzmann's constant, T is an absolute reference temperature, b is bandwidth in Hz measured in a short vertical antenna over a conducting ground plane. This is identical to the CCIR 322-3 [CCIR, 1988] scaling and was used in the final calibration of the NoiseProp program.

3.0 PROPAGATION OF RF NOISE FROM GLOBAL DISTRIBUTION OF LIGHTNING ACTIVITY: 60 kHz TO 20 MHz

As in the LNP ELF, VLF prediction code NoiseProp divides the globe into 10°×10° sectors. Each 10° × 10° sector is regarded as an equivalent noise transmitter (ENT). The long term median lightning flash rates computed from the ISS-b satellite GLO maps are sorted by 10°×10° sectors. The accumulation of individual noise transmitters is combined into a single effective radiator -- the ENT--and positioned at the center of mass of the sector. Typical flash rate data is shown in Figure 3-1. The power contributions from all worldwide ENTs are then summed to yield the total median noise power (at a particular receiver location). This procedure is the same whether GLO data or short term DGLO data are used. If DGLO data updates are only available over limited geographical areas, both GLO and DGLO maps will be used with the original long

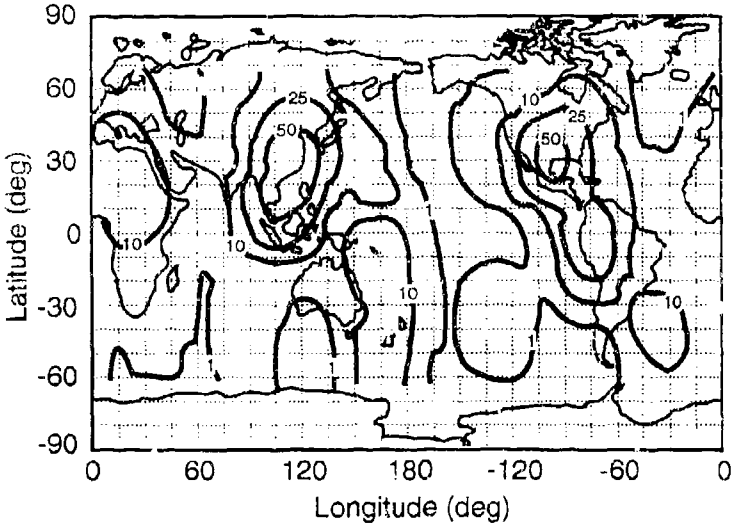

Note: Frequency of lightning discharges occurring within 100 km²/s is obtained by multiplying contour value by 10^{-6}.

Figure 3-1. Typical global lightning flash rate distribution. From June-July-August, 2200-0200 UT ISS-b satellite data.

term GLO maps replacing the DGLO maps where the latter are nonexistent. This method is illustrated in Figure 3-2 and the summation can be written

$$N(x,y) = \sum_{i=1} P_i(x,y) p_i n_i \quad , \tag{3.1}$$

where the summation is over all ENTs and

N N is the total noise power at receiver location (x,y) in a 1 Hz bandwidth

P_i is the power in watts of the i^{th} ENT

n_i is the number of flashes (in 1 s) represented by the i^{th} ENT

$P_i(x,y)$ is the propagation factor (loss) for the path from i^{th} ENT to the location (x,y).

The propagation factor $P_i(x,y)$, in principle, depends on the radiowave frequency, the great circle distance between the i^{th} ENT and the receiver position (x,y), and the complete geophysical description of the propagation path; namely, the ionospheric conductivity height possible, the

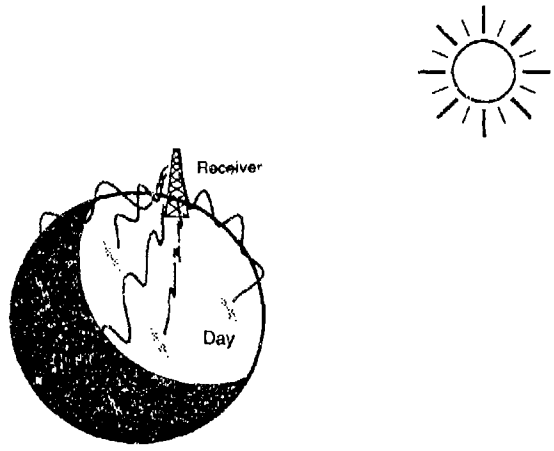

Figure 3-2. Noise model methodology: Equivalent Noise Transmitters (ENTs) and propagation paths to a receiver.

ground conductivity, and the geomagnetic field elements specified at each position along the path (at a particular time and season). P_i represents the propagation of one watt from the i^{th} ENT and $[P_i \cdot p_i]$ represents the propagation of the energy in one flash from the i^{th} ENT.

In the ELF, VLF regime (wavelengths ~ 10 to 1000 km) the path is subdivided into segments whose ionospheric, geomagnetic, and ground properties can be considered constant (or insignificantly varying on the scale of a wavelength). Each such segment then provides boundary conditions for the solution of an eigenvalue problem for the propagation constant (mode constant) in the model expansion for the transverse electric field in the earth-ionosphere waveguide [Davies, 1990; Budden, 1961; Warber and Field, 1991]. Modal expansions on each path segment are matched so as to satisfy certain boundary conditions (mode coupling) and the propagation is then complete. At ELF and VLF only a few modes are needed for an adequate expansion of the field. Mode constants for various earth/ionospheric/geomagnetic parameter values are precomputed and interpolated as needed, making the propagation algorithm fairly rapid and efficient.

The relative simplicity of the modal expansion breaks down above VLF and we must use alternate approaches to the solution of the propagation factor. At the MF and above (~100 kHz to 30 MHz) the wavelength is such that the ionosphere can be said to be a slowly varying medium with respect to a wavelength. The methods of geometrical optics are applicable for the determination of signal power by multiple ionospheric and ground hops (see illustration in

Figure 3-3). Geometrical optics and ray tracing methods for HF propagation have been developed for several decades and exist in various degrees of sophistication. They range in complexity from simplified engineering formulations originally used with charts and nomographs [CRPL, 1948] to full-blown shooting methods which trace rays through ionospheric profiles with realistic profiles and horizontal gradients [Hatfield and Smith, 1987]. Propagation losses are either accumulated using semi-empirical rules at each ionospheric hop (in the simpler methods) or accrued by analytically or numerically integrating the ionospheric refractive index along the ray path as it is traced (in the sophisticated methods). Naturally, what is gained in accuracy with the sophisticated ray tracing methods is usually lost in efficiency. These methods must perform time consuming iterations to find the exact ray solutions connecting a transmitter and receiver. Furthermore, the accuracy in such a method may be greater than the accuracy intrinsic to the underlying ionospheric model.

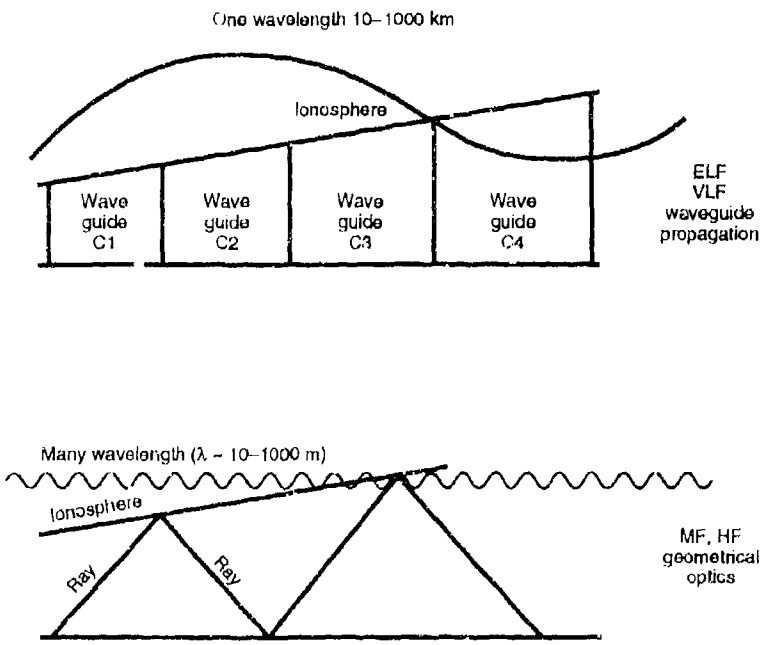

Figure 3-3. Wave guide propagation for ELF-VLF signals: ionospheric and geomagnetic properties vary significantly within one wavelength. Geometrical optics propagation for LF-MF-HF propagation: ionosphere can be considered slowly varying on the scale of one wavelength.

A commonly used approximate method for communications purposes is called the virtual ray trace method. In this method, the propagation path is divided, a priori, into a certain number of hops (depending on the path length and the ionospheric profile at one or more positions along the path). On each segment an appropriate takeoff angle and equivalent reflection height is determined by an empirical or analytic relationship between the hop length and ionospheric profile at the hop midpoint. Assumption of a special (e.g., parabolic) electron density profile facilitates analytic calculation [Barghausen et al., 1969]. The resulting set of independent hops are then combined into one geometrically self-consistent mode by a pass-range adjustment algorithm which guarantees equal takeoff angles on all hops.

After extensive investigation of the existing algorithms for HF (2 to 30 MHz) propagation, we developed a hybrid method which is a virtual ray trace method based on standard ionospheric maps, but is not burdened by the communications oriented overhead of the canonical programs, e.g., IONCAP. Indeed, in NoiseProp application, dozens or even hundreds of noise transmitters (ENTs) are propagated over a random assortment of paths and we would expect that subtle differences between several different propagation methods be washed out in the overall summation of energy. Therefore, computational expediency can be regarded as a priority of the first order. (Even as such, the method ultimately chosen is quite computationally intensive over a grid of many receivers.)

The method used in the LF-MF regime (60 to 900 kHz) is also a skywave wave hop method. It differs from that used at HF chiefly in a different ionospheric loss model (empirical reflection coefficients) and diffractive corrections required at the longer LF-MF wavelengths (but not at HF). Between 900 kHz and 2000 kHz a third empirical propagation algorithm was chosen. In this frequency range, the magnitude and direction of the earth's magnetic field becomes a more sensitive determinant of propagation then elsewhere. Accordingly a propagation algorithm specific to this upper MF band is employed in NoiseProp.

4.0 EXTENDING LIGHTNING SOURCE SPECTRA ABOVE 60 kHz

The original LNP source model consists of a hypothetical ENT located at the center of each $10°\times10°$ sector of the earth. The power radiated in a 1 Hz bandwidth by an ENT is

$$P = ESD * FR \quad \text{(watts)} \quad . \tag{4.1}$$

The ESD is the generic flash energy spectral density in units of Joules/Hz (or equivalently watts/HZ^2) and FR is the flash rate for the particular 10°×10° cell in units of sec^{-1}. The flash rate is determined directly from the long term satellite based GLO maps (or the short term meteorology based dynamic DGLO maps as they become available). The ESD must be derived from various lightning spectra measurements reported in the literature.

Typical lightning spectra measurements are made at distances of 10 to 50 km from a flash and are detected either by wide band receivers or banks of several narrowband receivers (tuned to different frequencies) [Uman, 1987; Weidman and Krider, 1986; Nanevicz, 1987; Willet et al., 1990]. When banks of narrow band receivers are used the spectrum of a flash can be plotted directly, but the resulting spectrum will be a sum of all flash constituents spectra (strokes) which occur within the averaging time of the narrow band filtering; stroke spectra within a flash cannot be individuated by narrow band measurements. Wide band receivers coupled to digital fourier analysis systems can, on the other hand, be used to find separately the spectra of the flash subprocess or strokes; namely, the return stroke (RS), stepped leader (SL), in-cloud (IC), etc. [Warber and Field, 1991].

Mathematically,

$$S(t) = \sum_{i=1}^{N} s_i(t - \tau_i) \quad (V/m) \ , \tag{4.2}$$

where S(t) is the measured electric field as a function of time of the entire flash and the s_i are the constituent strokes within the flash. The τ_i are the times at which the i^{th} stroke commences. We assume that the strokes within a flash do not overlap and that the τ_i are otherwise randomly distributed. It then follows that the flash spectrum is given by

$$\|S(f)\|^2 = \sum_{i=1}^{N} \|s_i(f)\|^2 \quad (V/m)^2 / Hz^2 \tag{4.3}$$

where, by definition

$$S(f) = \int_{-\infty}^{\infty} S(t) e^{2\pi i f t} dt \ . \tag{4.4}$$

Narrowband measurements tend to reproduce values of $\|S(f)\|^2$ directly, whereas a posteriori analysis of digitized wideband signals allows separate reconstruction of the individual stroke

spectra $\|S(f)\|^2$ i=1, ..., N. Corresponding to each s_i is an energy spectrum (ESD_i) and the ESD for the entire flash is the sum of the ESDs of the constituent strokes.

We show next that at medium and high frequencies (>100 kHz) the energy spectral density ESD is related to the flash spectrum by

$$ESD = \frac{d^2\|S(f)\|^2}{30} \text{ watts / Hz}^2 \qquad (4.5)$$

where d is the distance from flash to the observation point.

In a narrowband receiver the response due to radio frequency energy from a lightning flash is seen as an oscillation at the bandpass center frequency f which is amplitude modulated by a slowly varying envelope e(t).

$$E(t) = e(t) \bullet \sin(2\pi ift + \phi)dt \quad V / m \qquad (4.6)$$

Now letting

$$S(f) = \int_{-\infty}^{\infty} E(t)e^{2\pi ift}dt \qquad (4.7)$$

as above, we have

$$\int_0^{\infty} \|S(f)\|^2 df = \frac{1}{2}\int_{-\infty}^{\infty} E^2(t)dt \qquad (4.8)$$

$$\int_{-\infty}^{\infty} E^2(t)dt = \int_{-\infty}^{\infty} e^2(t)\sin^2(2\pi ft + \phi)dt = \frac{1}{2}\int_{-\infty}^{\infty} e^2(t)dt - \frac{1}{2}\int_{-\infty}^{\infty} e^2(t)\cos(4\pi ft + \phi)dt \qquad (4.9)$$

so

$$\int_{-\infty}^{\infty} E^2(t)dt \approx \frac{1}{2}\int_{-\infty}^{\infty} e^2(t)dt \ , \qquad (4.10)$$

since the last integral is vanishingly small when e(t) is slowly varying. Hence,

$$\int_0^\infty \|S(f)\|^2 df = \frac{1}{4}\int_{-\infty}^{\infty} e^2(t)dt \ . \qquad (4.11)$$

Letting BW denote the receiver bandwidth:

$$\|S(f)\|^2 = \frac{1}{4 \bullet BW}\int_{-\infty}^{\infty} e^2(t)dt \ . \qquad (4.12)$$

Now, at MF and HF it is appropriate to consider the lightning flash as an isotropic, randomly oriented radiator at approximately the cloud base height (2 to 7 km) [Uman, 1987; Horner, 1964; Kotaki, 1984]. If e(t) is the instantaneous envelope in V/m measured in a short vertical monopole at ground, the instantaneous power flux will be

$$\frac{e^2}{2Z_0} \equiv \frac{e^2}{240\pi} W/m^2 \ . \qquad (4.13)$$

We then integrate the isotropically distributed flux over a hemisphere of radius d (d is the horizontal distance from source to observer (d ~ 10 to 50 km) to obtain total instantaneous source power

$$P = \frac{e^2 d^2}{120} \ . \qquad (4.14)$$

The total energy in the flash (in the measurement passband) is $E = \int pdt$. Hence

$$E = \frac{d^2}{120}\int e^2(t)dt = \frac{d^2}{30} \bullet BW \bullet \|S(f)\|^2 \ \text{watt} \bullet \text{sec} \ , \qquad (4.15)$$

using Eq. (4.12) above.

Consequently, the mean power (using Eq. xx above) over the time T(sec) of the flash duration is (in bandwidth BW):

$$\langle P \rangle = \frac{d^2 \bullet BW \|S(f)\|^2}{30T} \ \text{watts} \qquad (4.16)$$

and the energy spectral density (ESD)

$$\mathrm{ESD} = \frac{d^2 \bullet \|S(f)\|^2}{30} \text{ watts / Hz}^2 \quad . \qquad (4.17)$$

In the LNP formalism, below 60 kHz, the ESD is built up from a weighted sum of dominant stroke spectra $\|S_i(f)\|^2$. These spectra $S_i(f)$ are found for return strokes and certain in-cloud radiators in articles by Weidman and Krider [1986]; Willet et al. [1990], Uman [1987]; and Greifinger [1989]. We have extended this decomposition of the overall flash ESD from 60 kHz up to 1 MHz, utilizing the same weighting as in LNP. In LNP, a typical flash will consist of four return strokes, 20 vertical in-cloud strokes, and 20 horizontal in-cloud strokes [Warber, 1991]. The number of strokes per flash is an adjustable parameter of the model. Above about 1 MHZ, however, the simple description of a flash as consisting of a small number of recurring basic stroke types becomes inadequate. Above 1 MHZ, a narrowband receiver's response to a lightning flash is significantly enhanced by a composite of hundreds or thousands of rapid intercloud discharges which are not strong radiators at VLF [Nanevicz, 1987; LeVine, 1987].

Hence, at HF, the combined spectra of return strokes, leader pulses, and the few other specific stroke types that have been separately analyzed in the literature cannot reproduce the spectral amplitude and slopes seen in typical narrowband receiver measurements. We have therefore used an empirical amplitude spectrum for the entire flash at frequencies above 1 MHZ [Horner, 1964; Kotaki, 1983, 1984]. Figure 4.1 shows the extension of the return stroke and bipolar (in-cloud) stroke spectra. The curves below 100 kHz are identical with those used in the original LNP model. Between 100 kHz and MHz, the return stroke spectrum and the bipolar spectrums are interpolated so as to join smoothly with the return stroke spectrum shown in Willet et al., [1990] above 1 MHz. The spectra in Weidman and Krider [1981, 1986] indicate that the bipolar in-cloud stroke spectra are essentially coincident with the return stroke at higher frequencies. Above 1 MHz the estimated flash spectrum of Horner [1964] shown by the straight line in Figure 4-1 is used instead of the LNP weighted combination of stroke spectra.

Due to the sparsity of published complete flash characterizations above VLF-LF, the spectral models in the NoiseProp model are inevitably a source of uncertainty in the final results, namely the noise at a given receiver location. A posteriori calibrations of the model output as a function of frequency must be made (see Section 11.0 under calibration).

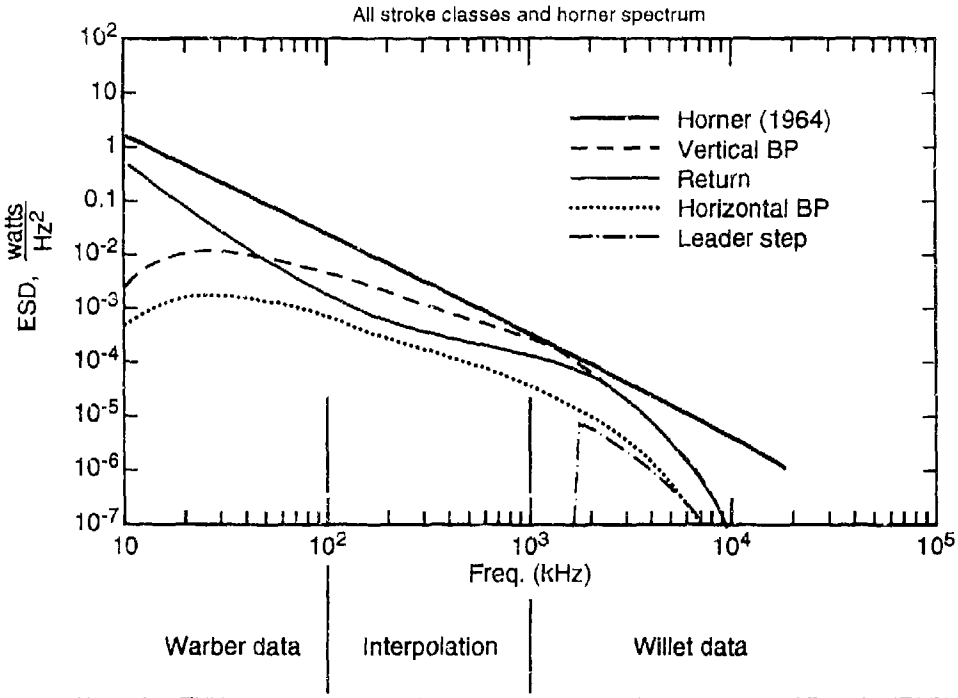

Figure 4-1. Extended ENT source spectra. Dimensions are that of Energy Spectral Density (ESD) in Watts/Hz/Hz (Joules/Hz). Return stroke spectrum is interpolated between the LNP spectrum and the spectrum of Willet [1990]. The vertical bi-polar spectrum is smoothly interpolated so as to join that of the Willet [1990] Return Stroke. The Horner [1964] complete narrow-band flash spectrum is also shown.

5.0 SUMMARY OF LF, MF PROPAGATION METHODS

Low frequency radio waves (30 to 300 kHz) are reflected at the lower side of the ionospheric D-layer (~70 km, day; ~90 km, night) and may propagate strongly over distances up to 1000 to 5000 km. Above 60 kHz (the upper limit of the LNP propagation capability) it becomes convenient to represent propagation as occurring along geometric hops defined by a set of ionospheric and ground reflections [Johler, 1962; CCIR, 1990]. This is referred to as the wavehop method.

Medium frequency (300 to 3000 kHz) propagation by D and E-layer reflection is strongly affected by the geometry of the earth's magnetic field since the electron gyro frequency (~0.8 to 1.6 MHz) always falls somewhere within this band. Moreover D-layer absorption of MF signals is quite pronounced. During daylight, distance skywave MF signals are very highly attenuated

and a local ground wave signal will dominate. Nighttime D-layer absorption is small, allowing long distance propagation. The complexity of a purely physical propagation model at MF is such that empirical or semi-empirical models are usually employed [Davies, 1990; PoKempner, 1980; CCIR, 1992b].

6.0 NOISEPROP LF PROPAGATION METHOD

Following CCIR 265-7 [CCIR, 1990] and Johler[1961] we have developed a wavehop method that allows calculation of the radiated field from a lightning source at frequencies from 60 kHz up to the middle MF band (500 to 900 kHz). The wavehop method is a geometrical-optics approximation with added diffraction corrections to account for the sphericity of the earth and ionosphere [Wait, 1960]. The algorithm divides the path between the ENT source and the receiver into a sequence of hops. This is accomplished by an exact geometric solution connecting an elevated source and a ground based receiver by up-going and down-going ray paths, allowing for the crossing of the day-night terminator. Day and night reflections are assumed to occur, to a first approximation, at 70 and 90 km, respectively, at lower frequencies (D-layer reflection) and at 105 and 110 km at higher frequencies (E-layer reflection). Figure 6-1 shows a schematic of a multihop day to night path. These reflection heights are interpolated as functions of wave frequency between 60 and 900 kHz.

Associated with each ionospheric reflection point is a 2×2 matrix of reflection (or transmission) coefficients describing the ratios of reflected and incident waves below the ionosphere of two orthogonal polarizations. The magnitudes of the reflection coefficients describe the attenuation of field strength incurred in an ionospheric reflection. The reflection coefficients can be obtained using an ionospheric model and integrating a coupled set of differential equations (equivalent to Maxwell's equations) for the field components E_x, E_y, H_x, H_y downward from a great height [Budden, 1961]. The reflection coefficients are formed from suitable combinations of these field components below the ionosphere. The reflection coefficients depend upon the ionospheric electron density and collision frequency profiles, the geomagnetic field direction and strength as well as the ray incidence angle and wave frequency. Determination of reflection coefficients in this manner is called a "full wave" calculation.

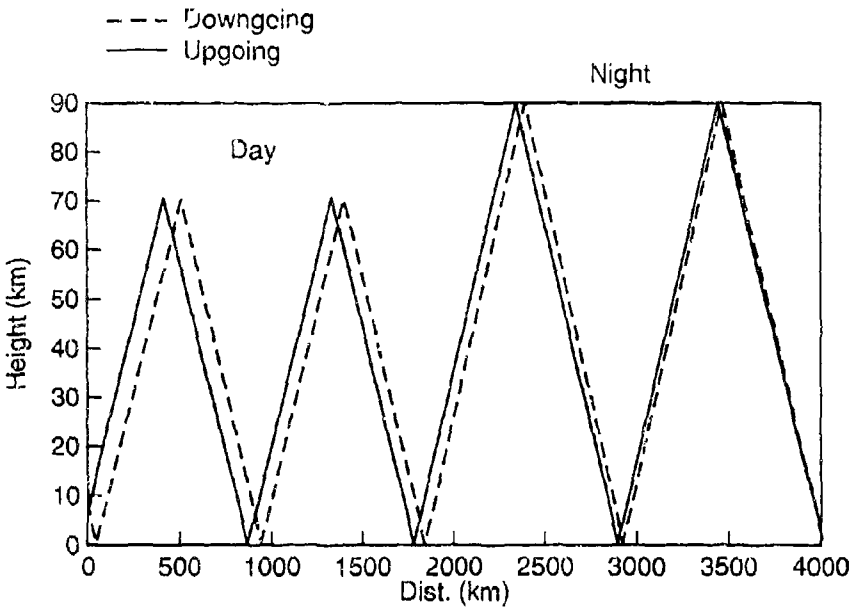

Figure 6-1. Schematic of the LF wave hop method ray path showing up- and down-going rays from a lightning source at ~6 Km. In this example the propagation path crosses the day-night terminator. At LF, D-layer reflections occur at nominal heights of 70 and 90 km for day and night, respectively.

In a full wave calculation four complex reflection coefficients (R_{11}, R_{12}, R_{21}, R_{22}) are obtained for each particular set of ionospheric and geomagnetic conditions, wave frequency, and incidence angle. Figure 6-2 shows typical nighttime reflection coefficients as a function of frequency. Rij is the ratio of a reflected plane wave of polarization j to an incident plane wave of polarization i measured below a planar, horizontally stratified magnetoionic medium; index 1 denotes vertical polarization (magnetic vector transverse to plane of propagation), index 2 denotes horizontal polarization (electric vector transverse to plane of propagation). The four Rij determine a matrix $R = \begin{bmatrix} R_{11} & R_{12} \\ R_{21} & R_{22} \end{bmatrix}$. For multiple hop propagation, the overall reflection coefficient will be the matrix product $R^N = R_N G_{N-1} R_{N-1} G_{N-2}, \ldots, R_2 G_1 R_1$ where the matrices $G = \begin{bmatrix} G_{11} & 0 \\ 0 & G_{22} \end{bmatrix}$ are the fresnel reflection coefficients for the intermediate ground reflection points. In particular, the magnitude $\|R_{11}^N\|$ of the 1,1 component of the product matrix RN gives the overall path loss (due to reflections) for a vertical electric dipole transmitter (VED) and a

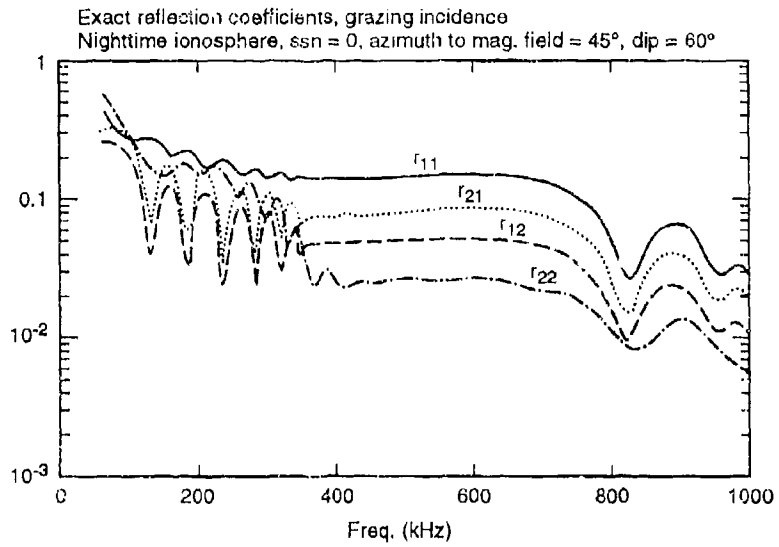

Figure 6-2. Typical nighttime ionospheric reflection coefficients computed by full wave integration [Budden, 1961] shown as a function of wave frequency for grazing ionospheric incidence (about 80) and fixed magnetic dip and declination angles (low solar activity).

VED receiver separated by N ionospheric reflections and N-1 intermediate ground reflections. Then the electric field of this N hop mode will be

$$E_N = K \cdot D_N^{-1} G_N^t G_N^r \cdot \alpha_N \cdot F_N \cdot R_{ij}^N \quad V/m \tag{6.1}$$

where

- K is a proportionality constant depending on the transmitter power in watts (the ENT power)
- D_N is the physical length of the N hop ray connecting source and receiver in km
- G_N^t, G_N^r are the transmitter and receiver antenna gain patterns, e.g., for simple vertical electric dipole $G_{ij}^N = \cos\psi_N$ where ψ_N is the takeoff angle of the N hop ray.
- R_{ij}^N is the i,jth component of the ov all N hop reflection coefficient matrix for source polarization i and receiver polarization j.

α_N is the convergence correction discussed in Wait [1960] and Johler [1961] which converts the plane wave reflection coefficient R^N into an effective spherical reflection coefficient.

$$\alpha_N = \left(1+\frac{h}{a}\right)\left[2N\sin\frac{\theta}{2N}/\sin\theta\right]^{1/2}\left\{\left[a\left(1-\cos\frac{\theta}{2N}\right)+h\right]/\left[(a+h)\cos\frac{\theta}{2N}-a\right]\right\}^{1/2} \bullet A_N$$

$$A_N = \left[\frac{\pi}{2}Z_N\right]^{1/2} H_{1/3}^{(2)}[Z_N]\exp\left[-i\left(\frac{5\pi}{12}-Z_N\right)\right]$$

h = reflection height (effective ionospheric reflection height)

a = radius of earth

θ = [transmitter-receiver distance]/[radius of earth]

Z_N = $\omega/c \sin^3\psi_N/3\cos^2\psi_N$

ω = angular wave frequency

c = speed of light

ψ_N = N hop ray takeoff angle

$H_{1/3}^{(2)}$ = is the Hankel function of order 1/3, of the second kind [Abramovitz and Stegun, 1972; Cambridge Computational Laboratory, 1945].

F_N is the cutback factor discussed in Wait and Conda [1958] which accounts for the presence of the earth at both transmitter and receiver. In the geometrical optics region this may be written

$$F_N = \left[1+R_i^1(\psi_N)\right]\left[1+R_j^1(\psi_N)\right] \qquad (6.2)$$

$R_{i,j}^N$ are the fresnel plane reflection coefficients of the ground at the source and receiver, takeoff angle ψ_N, source and receiver polarization i and j. A ground conductivity map indicating land and water regions of the earth is used.

We compute the electric intensity due to a single lightning flash as the RMS sum

$$E_{RMS} = \left[\sum_{N=1}^{M}\left\|E_N\right\|^2\right]^{1/2} V/m \qquad (6.3)$$

(over some sufficient number of hop models m - presently m = 4) for both up- and down-going rays emanating from an elevated isotropic point source (the ENT).

A ground wave computation is also performed on the closest lightning sources only (local storms) and the squared magnitude of the ground wave is summed with the geometric ray modes above. (see Section 9.0 below)

To facilitate practical computations we constructed a data base of precomputed reflection coefficients by repeatedly integrating the coupled field equations [Budden, 1961] through model daytime and nighttime ionospheres (under both high and low sunspot conditions) based on the IRI-90 ionosphere in Bilitza et al., [1990]. Figure 6-3 shows model day and nighttime D and E layers from IR-I90. The computations were performed for 10 wave frequencies between 60 and 900 kHz; 10 incidence angles between 1 and 80°; 8 values of magnetic field azimuth (with respect to propagation direction) between -90 and 225°; 7 values of geomagnetic field co-dip angle between 0 and 180° (the electron gyrofrequency was fixed at 1.3 MHz). The resulting data base serves as the skeleton for a four-dimensional linear interpolation procedure to obtain reflection coefficients for day, night, high or low sunspot activity for any combination of frequency, incidence angle, magnetic azimuth, propagation direction, and co-dip angle. Figure 6-4 compares the exact and interpolated reflection coefficient as a function of frequency.

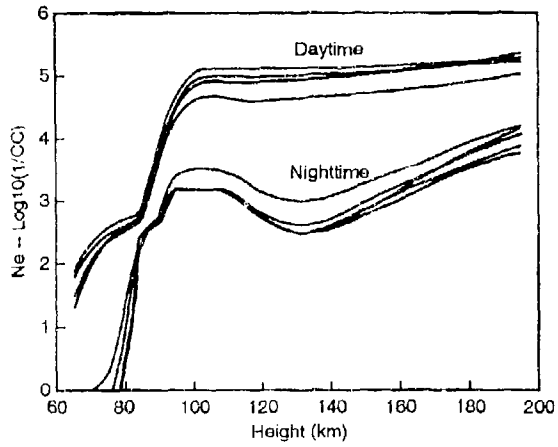

Figure 6-3. Typical day and nighttime ionospheric D and E-layer profiles from the IRI-90 model ionosphere. Profiles shown are for a variety of geographic latitudes and are averaged over season.

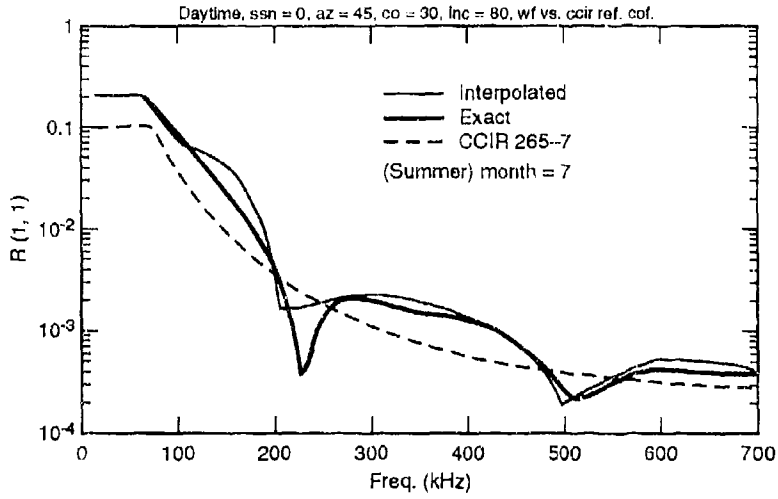

Figure 6-4. Comparison between full wave daytime ionospheric reflection coefficients and coefficients interpolated from pre-computed database (see text). Also shown is the empirical data from CCIR Report 265-7 [CCIR, 1990].

The CCIR Report 265-7 [CCIR, 1990] contains graphs of empirical values of the reflection coefficient R_{11} (vertical source and receiver polarization) as a function of wave frequency and ionospheric ray incidence angle (the functional dependence is on $f \cdot \cos(i)$). Curves are given for all seasons, nighttime ionosphere, and a separate summer and winter daytime set. Also given are curves which indicate the variation in reflection coefficient magnitude from solar minimum to solar maximum conditions. These data shown in Figure 6-5 were based on numerous propagation measurements in which oblique incidence ionospheric reflection losses were inferred from skywave-groundwave interference. The CCIR reflection coefficients, being averages over many propagation paths, do not have explicit dependence on magnetic field direction. We found, however, that there was good agreement between the precomputed fullwave reflection coefficients and the CCIR curves which we digitized and implemented in a computer program especially for the case of grazing incidence. Figure 6-6 shows a typical comparison.

From the standpoint of computational efficiency in the NoiseProp program, utilizing the CCIR reflection coefficients instead of the fullwave coefficients (which still require a 4D interpolation and magnetic field evaluation at every ionospheric reflection area) provides a significant

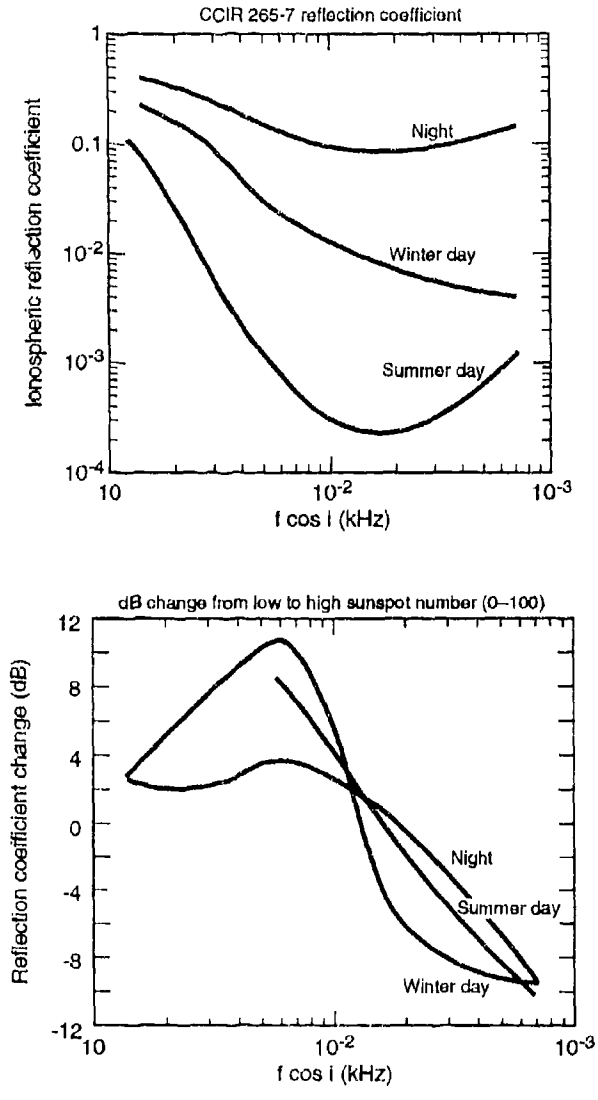

Figure 6-5. CCIR Report 265-7 empirical reflection coefficients and adjustment for solar activity. The nighttime curves are for all seasons; the daytime curves are grouped into two six-month seasons. The independent variable is F cos(i) where F is the wave frequency in kHz and i is the incidence angle at the ionospheric D layer.

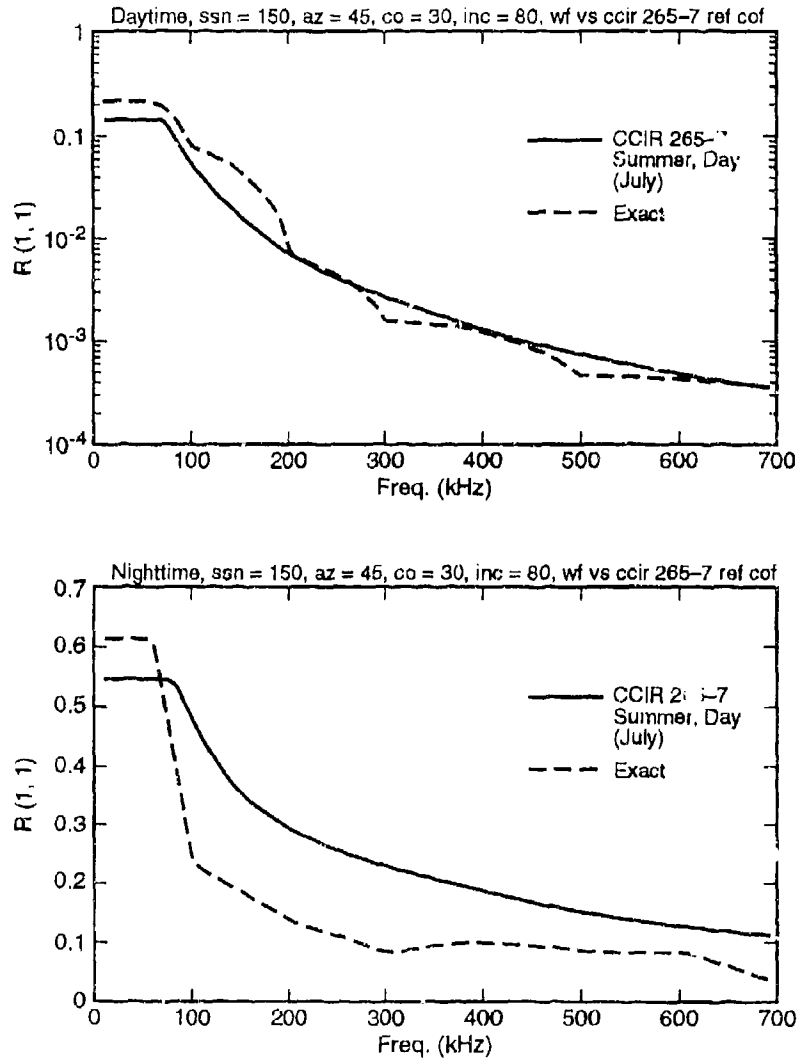

Figure 6-6. Typical comparison between the CCIR 265-7 empirical reflection coefficients and the full wave (exact) computations. Grazing ionospheric incidence, day and nighttime ionospheres, high solar activity.

computation time savings. Since the NoiseProp program sums noise propagated over hundreds of different paths to the receiver, it appears that the averaged-out aspect of the CCIR reflection coefficients has a minimal effect on the overall combination of path losses. We have retained both the fullwave and CCIR reflection coefficients but the present implementation of NoiseProp has been calibrated using the faster CCIR reflection coefficient calculation in the LF propagation section.

7.0 MF PROPAGATION METHOD (~900 kHz to 2 MHz)

At frequencies above ~900 kHz and low takeoff angles (corresponding to ~2000 km hop lengths) the CCIR 265-7 reflection coefficients no longer are applicable. Moreover, the complicated effects inherent in MF propagation (the sensitive role of the geomagnetic field direction and magnitude; and significant short-term, day to day, diurnal, seasonal, geographical, and solar cycle variations in ionospheric loss) make a simple, physical model (such as the wave hop method) underdetermined in both the number and scope of the contributing physical phenomena which can be modeled.

Various techniques have been developed to model MF propagation [PoKempner, 1980]. We have chosen a relatively simple empirical method published by the CCIR as Recommendation 435-7 [CCIR, 1992b]. Method 435-7 was based on statistical analyses of field strength measurements for 266 propagation paths distributed worldwide; as well as analysis of separate areas for which propagation paths were unavailable. This type of method is usually derived from a multiple regression analysis of monthly median field strength measurements from which the dependencies on variables such as frequency, path length, solar activity, geomagnetic field vector at intrapath control points, solar zenith angle, etc. are determined. The predicted skywave field strength (vertical polarization) is given by:

$$E = V + G_s - L_p + A - 20\log_{10} p - 10^{-3} K_R P - L_t \qquad (7.1)$$

where

E is the annual median of half-hourly median field strength in dB (μV/m)

V = P + G, where P is the radiated source power in dB/(1 KW) and G accounts for transmitting antenna elevation and azimuth gain and efficiency (dB)

G_s is the sea gain correction important only when the transmitter or receiver is near seawater

L_p is the polarization coupling loss (dB)

$$L_p \equiv 180\left[36 + \theta^2 + I^2\right]^{-1/2} - 2$$

where θ is the path azimuth in degrees from the geomagnetic E-W direction, $|\theta| \leq 90°$, I is the geomagnetic dip angle, L_p is evaluated (using a 13 coefficient expansion for magnetic dip and declination) at both source and receiver locations and the results added.

A 106.6 - 2sinΦ where Φ is a path averaged value of geomagnetic/latitude.

P is the slant path length for E-layer reflections approximately $(d^2 + 40{,}000)^{1/2}$ where d is the path great circle distance in km.

K_R is the loss factor, $K_R = 3.2 + 0.19f^{.4} \tan^2(\Phi + 3) + 0.01 \bullet b \bullet SSN$

where f is the frequency in kHz, SSN is the 12 month running average sunspot number, b = 4 for North American paths, 1 for European and Australian paths, and 0 elsewhere.

L_t is the diurnal loss factor.

The method depends on graphs contained in CCIR report 435-7 [CCIR, 1992b] for the sea gain Gs and diurnal loss term Lt. Furthermore, rather involved averaging rules are given for the determination of a single value of the geomagnetic latitude Φ to use for paths up to 12000 km. The algorithm was computerized by Inuki et al. [1983] and validated against observations. It is, of course, also intrinsically consistent with the CCIR path data base used to derive it. We have programmed a slightly simplified version of the algorithm, similar the summary given in Davies [1990, pp. 433-436]. We use the algorithm with its weak $f_{kHz}^{.4}$ loss dependence up to 2000 kHz. Above 2000 kHz an HF propagation method is implemented. As in the LF section, the NoiseProp algorithm sums MF power radiated by using 250 lightning ENT sources.

8.0 NOISEPROP HF PROPAGATION METHOD

HF propagation predictions, unlike LF and MF, require a comparatively detailed ionospheric description. Above 2 MHz, the NoiseProp program performs ionospheric propagation

calculations using empirical E and F2 layer numerical maps in combination with algorithms describing the takeoff angle and virtual reflection height of ray paths from source to receiver. The propagation algorithm is based on the CCIR Recommendation 533-3 [CCIR, 1992c] method though there are certain significant differences in our approach. The description of the ionospheric F2 layer parameters, foF2, M(3000)F2, hmF2 are those used in the International Reference Ionosphere IRI-90 [Bilitza, 1990] and the CCIR Recommendation 434-5 [CCIR, 1992a]. This F2 layer description is the so-called CCIR "Oslo" ionosphere [CCIR, 1966, 1967] represented by 12 monthly 15 coefficient fourier series diurnal variation and a spherical harmonic expansion in terms of the modified dip angle, arctan $\left[I / \sqrt{\cos\phi}\right]$, where I is the geomagnetic dip angle and ϕ is the geographic latitude. The model is linearly interpolated for sunspot numbers between 0 and 100. The E layer critical frequency, foE, is also based on the formulation used in IRI-90 and CCIR 434-5 [CCIR, 1992a].

The propagation model then determines several ray paths connecting the source to the receiver as follows:

- The great circle path (short path) between the ENT source and receiver is determined and divided into equal subsegments, one per hop. The maximal hop length is determined with respect to the F2 layer maximum height, hmF2 at midpath and will usually be approximately 4000 km.
- For each subsegment a one hop mode is sought as follows:
  - An F2 mode is first sought by utilizing the foF2, FoE, hmF2 data corresponding to the given universal time, month, and sunspot number at the segment midpoint (or averaged over the midpoint values and values at the adjacent points a quarter hop on either side).
  - An equivalent triangular reflection height (equivalent virtual height) is determined using the empirical algorithm described in CCIR 533-3. The empirical algorithm is used in place of the slower iterative procedure which solves the transmission equations for a double layered parabolic ionosphere to determine ray takeoff angle and virtual height as a function of path length [CCIR, 1986]. The algorithm determines virtual height as a function of frequency, hop length, and the state of the ionosphere (E and F layers) along the hop segment.
- The elevation angle thus determined for an F2 hop is tested for viability. In this case, we check to see if the takeoff angle is positive. If not, the hop segment is subdivided and the

process repeated until an F2 mode of positive takeoff angle is found for each path subsegment.

- The F2 mode on each subsegment is tested for E layer reflection. If the E layer critical frequency at the midpoint of any path subsegment is sufficiently high, foE > f/1.05 secϕ, where f is the wave frequency and ϕ is the ray incidence angle at 110 km. The F2 mode is completely occulted by the E layer. In this case the F2 hop on this subsegment is replaced by one or more E hops with virtual reflection height at 110 km.
- At this stage the path from the source to receiver has been subdivided into E and F layer hops. The E and F layer MUF (maximum usable frequency) are determined using the empirical methods in CCIR 434-5 [CCIR, 1992a] and CCIR 533-3 [CCIR, 1992c]. These are used to formulate a circuit MUF. In communications prediction, the circuit MUF is used to determine a circuit availability percentage. In our NoiseProp application, the circuit MUF is used to determine to determine an "above the MUF loss" term used in the subsequent propagation loss budget.
- The pass ranges and virtual reflection heights are sent to an adjustment algorithm. Here, the virtual heights are fixed, while the pass ranges are adjusted so that incident and reflected ray angles are equal at each ground reflection point. This adjustment forces the complete mode to be geometrically consistent and provides an adequate approximation to an exact physical solution. The exact solution relating the takeoff angle of a ray connecting a receiver and transmitter (separated by multiple hops spanning varying ionospheric conditions) to the total distance spanned can only be found by a time consuming iterative ray tracing search (shooting). In principle, the adjusted pass ranges could be returned to the virtual height algorithm, new virtual heights and takeoff angles determined, and the resulting ranges and ranges sent to the adjustment algorithm resulting in a uniform takeoff angle close to the true solution. This iteration would converge to the exact physical solution. The accuracy of the first adjustment is sufficient, however, for all communications oriented predictions and therefore the NoiseProp ENT propagation model as well. The adjustment is illustrated in Figure 8-1.

The median RMS field strength from a single ENT source in dB above 1 μV/m is the root-sum-square of individual modes:

$$E_{TOT} = 10 \cdot \log_{10} \sum_{k=1}^{M} 10^{(E_k/10)} \qquad (8.1)$$

a. Before adjustment

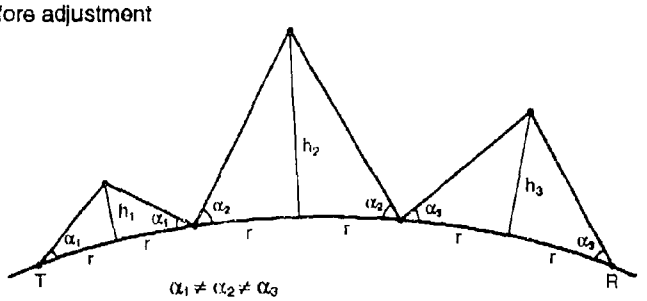

b. After adjustment

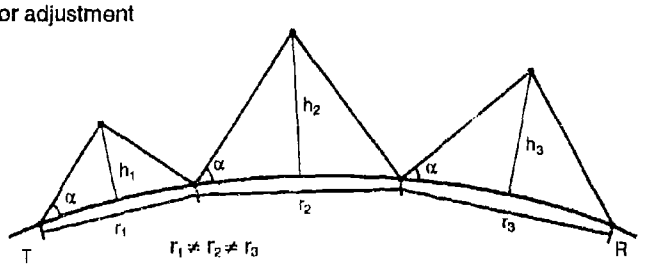

Figure 8-1. Pass-range adjustment in HF virtual raytrace propagation algorithm. Virtual heights are unchanged from a.) to b.).

where E_K is the median RMS field strength of the K^{th} multihop mode (in dB/1μV/m) and

$$E_K = 107.2 + 20\log_{10} f(\text{MHz}) + P_{ENT} + G(\alpha) - L(\alpha) \qquad (8.2)$$

where

- f = wave frequency in MHz
- P_{ENT} = ENT source power in dB above 1 watt
- α = the adjusted elevation angle of the mode
- $G(\alpha)$ = source gain at elevation angle α (dB)
- $L(\alpha)$ = propagation loss of K^{th} mode

Presently, the ENT source is modeled as an isotropic radiator and so $G(\alpha) = 0$. $L(\alpha)$ accounts for all losses accrued by the mode along its path. This term is composed of the following parts:

$$L(\alpha) = L_{bf} + L_{abs} + L_{gnd} + L_{pol} - G_{hf} - G_{lp} + L_{exl} + L_{MUF} \qquad (8.3)$$

- L_{bf} is the basic free-space loss due to the inverse distance falloff of the electric field magnitude. $L_{bf} = 20 \log_{10}[4\pi\rho'/\lambda]$ where ρ' is the ray path length and λ is the wavelength. In kilometer and mHz units: $L_{bf} = 32.45 + 20 \cdot \log f + 20 \log \rho'$.

- L_{abs} is the non-deviative absorption loss due to D and E layer transits. There are various empirical models which reduce the total absorption so a sum of terms, one per hop, or one per control point e.g., CCIR 533-3 [CCIR, 1992c], Barghausen et al. [1969], Lloyd et al. [1978], Fricker [1987], and Sailors and Rose [1993]. All the empirical methods except for that developed by the BBC [Fricker, 1987] are control point methods and average absorption only over 4 to 5 control point locations. Our virtual ray trace, however, depends explicitly on the ionospheric conditions from hop to hop. We therefore use the BBC absorption formula which explicitly sums the ionospheric absorption from each leg of each hop

$$L_{cabs} = \sum_{L_{legs}} 13 \bullet \Phi_n \frac{(foE)^2 \sec i_E}{(f+0.6)^2} \qquad (8.4)$$

where the sum is over up and downgoing legs of all hops, foE is the E-layer critical frequency at the point of intersection of the ray and 115 km altitude, i_E is the incidence angle of the unrefracted ray at 115 km ($\left(i_E \cong \cos^{-1}\left(1 - 0.965\cos^2\alpha\right)^{1/2}\right)$ and Φ_n takes into account the depth of penetration of the ray. For an F2 hop

$$\Phi_n = 1 + \frac{0.07}{\left(\frac{f}{foE \sec i_E} - 0.75\right)^2} \qquad (8.5)$$

For an E-layer hop

$$\Phi_n = \frac{1.2}{\left(1.6 - \frac{f}{foE \sec i_E}\right)} - 0.41 \; . \qquad (8.6)$$

It is assumed that E-layer reflection occurs when

$$\frac{f}{foE \sec i_E} < 0.95 \; .$$

- L_{gnd} is the loss due to ground reflection on multi-hop modes. A 1° × 1° land-water map is used to determine the relative dielectric constant and conductivity ε_r, σ at each ground reflection point (seawater: $\varepsilon_r = 80$, $\sigma = 5$; land: $\varepsilon_r = 0.4$, $\sigma = 0.001$). The Fresnel reflection coefficients for vertical and horizontal polarization are computed

$$R_v = \left[n^2 \sin\alpha - \left(n^2 - \cos^2\alpha\right)^{1/2}\right] / \left[n^2 \sin\alpha + \left(n^2 - \cos^2\alpha\right)^{1/2}\right] \qquad (8.7)$$

$$R_H = \left[\sin\alpha - \left(n^2 - \cos^2\alpha\right)^{1/2}\right] / \left[\sin\alpha + \left(n^2 - \cos^2\alpha\right)^{1/2}\right] \qquad (8.8)$$

where $n^2 = \varepsilon_r - i(18000\sigma)/f$ MHz is the complex refractive index of the ground, α = ray takeoff angle. Then, assuming random polarization of the downgoing wave (a valid assumption for a ray after one or two ionospheric transits) we set the ground loss

$$L_{gnd} = 10 \bullet \log_{10}\left[\frac{\|R_v\|^2 + \|R_h\|^2}{2}\right]. \qquad (8.9)$$

- L_{pol} is the polarization coupling loss due to the imperfect coupling between the initial wave polarization and the two characteristic polarizations preferred by the ionosphere (X and O). We use a simple empirical formula described in Sailors and Rose [1993]:

$$L_{pol} = A + B \bullet (\text{average hop length in radians}) + N\text{hops}$$

where

$A = (2.400 \bullet N_E + 2.060 \bullet N_F)/N$ hops
$B = (2.548 \bullet N_E + 1.019 \bullet N_F)/N$ hops
N_E = number of E hops
N_F = number of F hops.
N hops = $N_E + N_F$

- L_{exl} is the excess system loss from the tables in Barghausen et al. [1969], CCIR 252-2 and 533-3 [CCIR, 1986; 1992c]. This empirical term allows for auroral and other high latitude losses. It is evaluated in terms of midpath geometric latitude (N or S of equator), season, and midpath local time and is 0 for geometric latitudes less than 42.5° (also see Lloyd et al., 1978).

- L_{MUF} is the "above the MUF" loss. The model does not assume that propagation ceases above the geometrical optics path MUF (junction frequency). It is known that the signal does not fall completely to zero at frequencies above the MUF. CCIR 533-3 [CCIR, 1992c] gives the following

for E modes
$$L_{MUF} = \left\{ \begin{array}{c} 0 \text{ if } f \le E\,MUF \\ \min\left(81dB, 130 \bullet \left[\frac{f}{E\,MUF} - 1 \right]^2 \right) \end{array} \right\} \qquad (8.10)$$

for F modes
$$L_{MUF} = \left\{ \begin{array}{c} 0 \text{ if } f \le F\,MUF \\ \min\left(62dB, 36 \bullet \left[\frac{f}{F\,MUF} - 1 \right]^{1/2} \right) \end{array} \right\} \qquad (8.11)$$

These empirical curves account for both 1) the effect on the median monthly field strength due to the source frequency exceeding the daily MUF on some days and not propagating, and 2) losses occurring (due to phenomena other than simple two-dimensional ray optics) on days when the source frequency is above the basic MUF but propagation occurs nonetheless (due to non-classical or non-ray optics phenomena).

- G_{hf} is a horizon focus gain for short paths (less than 1/4 of the earth's circumference, ~10,000 km). It is a polynomial fit (in elevation angle) to curves based on double parabolic E, F layer ionospheres. It reaches a maximum of 9 dB at small takeoff angles as shown in Figure 8-2. The curves are given by Sailors and Rose [1993]:

$G_{hf} = \sum_{i=0}^{6} a_i x^i$ for elevation angles $\le 10°$, x = (elevation angle -5°)/5°,

$G_{hf} = \sum_{i=0}^{6} b_i y^i$ for elevation angles $>10°$, y = (elevation angle -50°)/40°,

and the coefficients are given by

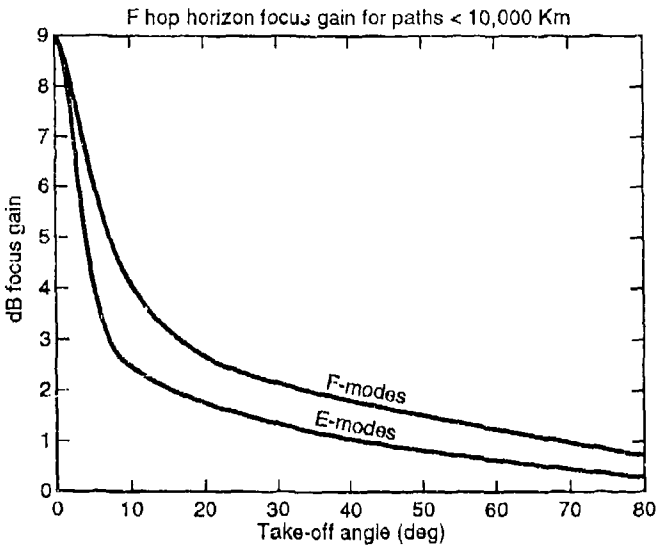

Figure 8-2. Horizon-focus gain for E and F-layer reflections as a function of take-off angle.

	a_0	a_1	a_2	a_3	a_4	a_5	a_6
E-modes	4.14	-4.00	3.007	0.069	-1.06	0.681	-0.347
F-modes	6.03	-3.161	1.400	0.624	-1.413	0.088	0.533

	b_0	b_1	b_2	b_3	b_4	b_5	b_6
E-modes	0.81	-0.876	0.353	-0.028	-0.227	-0.274	0.387
F-modes	1.50	-1.2444	0.173	0.540	-0.267	-1.136	0.853

- G_{lp} is a long path focus gain which is effective for circuit lengths greater than 1/4 of the earth's circumference and is given by

$$G_{lp} = 20 \log_{10}\left|1 - \frac{6371\pi}{D}\right|$$

where D is the circuit path length in km (always less than one-half the earth's circumference) [Hortenbach and Rogler, 1979].

8.1 Influence of Geomagnetic Activity

Extensive studies have shown that the F2 layer maximum critical frequency foF2 and the F2 layer MUF are significantly correlated with measured values of the local geomagnetic k-index [Davis, 1970; Wrenn and Rodger, 1989]. Two tendencies have been noted during periods of increased geomagnetic activity 1) a relative reduction of foF2 at auroral latitudes in summer or during high sunspot activity in local daytime, and 2) a relative enhancement of foF2 at low geomagnetic latitudes (above 35°) in winter or during low sunspot activity in the local afternoon and night. At middle latitudes these two tendencies are combined to a degree depending on the particular geomagnetic latitude, local time, and season.

Barghausen et al., [1969] used the results of Davis [1970] to adjust a given path MUF by a fraction P = (actual MUF)/(monthly median MUF) for a given local time and geomagnetic activity index. The fraction P is given by a linear regression on geomagnetic activity index k:

$$P = P_0 + b\,k \qquad (8.12)$$

where Po and b are coefficients which depend on geomagnetic latitude at midpath, three levels of sunspot number, three seasons, and eight local time blocks. The coefficients are linearly interpolated in sunspot number. The coefficient of correlation c from the regression analysis is also stored and the adjustment Actual MUF = P • (monthly median MUF) is only made for conditions where $|c| > 0.3$.

The adjustment of the path MUF for k index will affect the above-the-MUF loss term L_{MUF} in the propagation loss budget, particularly for propagation paths which cross high geomagnetic latitudes. In the NoiseProp summation over multiple ENT sources, the effect of the adjustment is probably only seen at high latitudes when the frequency is marginally greater than the path MUF for a majority of paths between the dominant ENT sources and the receiver. The k index adjustment can be defeated altogether in the NoiseProp inputs; in which case the MUFs and the corresponding L_{MUF} loss terms will all represent median conditions.

9.0 GROUNDWAVE PROPAGATION OF LOCAL ENTs

For local lightning ENT sources (closer than ~500 km to the receiver) we must consider propagation by the groundwave. The groundwave field derives from the solution to the wave equation over a smooth, finitely conducting spherical earth. The source will be a vertical electric dipole at an elevated point height h above the surface. The VED is the most efficient exciter of the vertically polarized groundwave . (An HED can also excite a groundwave but it will be orders of magnitude weaker and irrelevant from the standpoint of our NoisePro summation of ENT power.) Groundwave propagation is most efficient at lower frequencies, shorter distances, and higher ground conductivities.

The vertical electric field at great circle distance $d = a \bullet \theta$ measured along the earth's surface [Wait, 1970, 1974; Bremmer, 1949] is

$$E = E_0 \bullet W \tag{9.1}$$

where E_0 is the unattenuated field of a VED over a flat perfectly conducting plane and W is the groundwave attenuation function. These may be written

$$|E_0| = \frac{300}{d_{km.}} \sqrt{P_{kw}} \ V/m \tag{9.2}$$

and

$$W = \left(\frac{\theta}{\sin\theta}\right)^{1/2} \bullet \left(\frac{\pi x}{i}\right)^{1/2} \sum_{s=1}^{\infty} \frac{\exp(-ixt_s)}{t_s - q^2} \frac{w_1(t_s - y_1)}{w_1(t_s)} \frac{w_1(t_s - y_2)}{w_1(t_s)} \tag{9.3}$$

θ = d/a , (a = 6371 km)

k = 2π/(wavelength)

q = $-i(ka/2)^{1/3} \bullet \Delta$

$y_{1,2}$ = $2/ka)^{1/3} \bullet kh_{1,2}$, h_1 = source height, h_2 = receiver height

Δ = relative surface impedance

$$= \frac{k}{k_2}\sqrt{1-\left(\frac{k}{k_2}\right)^2}$$

$$k_2 = k \bullet \sqrt{\varepsilon_r - i \bullet 18000 \bullet f\,MHz \bullet \sigma}$$

ε_r = relative dielectric constant (ground)

σ = ground conductivity

$i = \sqrt{-1}$.

$t_s = t_s(q)$ are roots of the differential equation

$$\frac{dt_s}{dq} = \frac{1}{t_s - q^2}$$

with the initial condition

$$t_s(0) = Ai'(-\alpha_s)e^{-i\pi/3} \quad s = 1,2,3,\ldots,$$

where the α_s satisfy $Ai(\alpha_s) = 0$ s=1,2,3,..., and Ai(z) is the standard Airy function.

$\frac{w_1(t_s - y_1)}{w_1(t_s)}$ and $\frac{w_1(t_s - y_2)}{w_1(t_s)}$ are the height gains for the source and receiver. Since the receiver is on the ground, $y_2 = 0$ and we replace the second height gain factor by 1 and $w_1(t) = \sqrt{\pi}[Bi(t) - i(Ai(t)]$ where Ai(t) and Bi(t) are the standard airy functions [Abramovitz and Stegun, 1972].

The expression for the spherical earth attenuation function W reduces in the case $h_1 = h_2 = 0$ and d/a << 1 to the Sommerfeld flat earth attenuation function F(p) where

$$F(p) = 1 - i(\pi p)^{1/2} e^{-p} \operatorname{erfc}(ip^{1/2}) \text{ and } p = -i(kd/2)A^2. \qquad (9.4)$$

Groundwave propagation curves for a 1 kw source at ground level for frequencies from 15 kHz to 5 MHz have been plotted in Figure 9-1 for comparison with the unattenuated perfectly conducting ground dipole propagation (top curve). The higher frequencies are strongly attenuated beyond a few hundred kilometers.

The NoiseProp system only utilizes the groundwave algorithm for local sources which we define to be those within the same $10° \times 10°$ contour plot of flashrate density. Each subcell is assigned a flashrate density in accordance with that weighting scheme. The ENT radiated power derived from these $5° \times 5°$ sources is then propagated by the groundwave formalism to the receiver (using the geometric mean ground conductivity and dielectric constant along the path) and the received powers summed.

propagated by the groundwave formalism to the receiver (using the geometric mean ground conductivity and dielectric constant along the path) and the received powers summed.

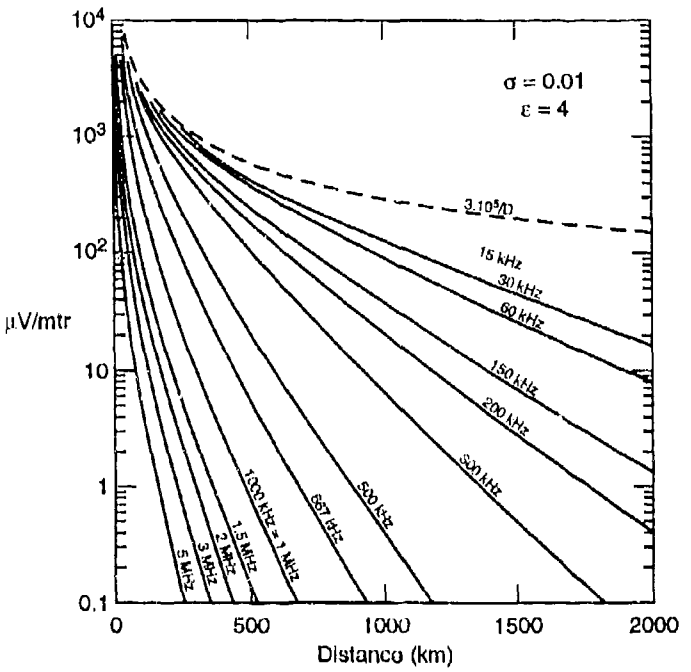

Figure 9-1. Ground wave signal strength in micro volts-per-meter over average (spherical) earth for a 1 kilowatt vertical electric dipole (VED) at ground level. Dashed curve shows 1/D falloff for 1 kW dipole over a perfectly conducting plane surface.

10.0 NOISEPROP PROGRAM AND POWER SUMMATION

10.1 Summary

Given a frequency (between 60 kHz and 30 MHz), a date (year, month, day), universal time, sunspot number, and receiver location, the NoiseProp program determines the noise factor Fa in decibels relative to kTb (k-Boltzmann's constant, T is 288°K, b is effective receiver noise bandwidth in Hz) in a short vertical monopole over a conducting ground plane. This figure can be computed for a percentage of time between 0.001 and 99.999%.

The NoiseProp program operates in a series of steps illustrated in Figure 10-1.

1. The appropriate seasonal and diurnal GLO maps (or DGLO maps if available) are converted into corresponding source power maps or ENT maps.
2. A sorting algorithm arranges the globally distributed ENT maps in a rough dominance ordering.
3. Depending on frequency, the appropriate propagation algorithm (LF, MF, HF) is applied repeatedly to each ENT source in order of dominance. The available power in the vertical electric field at the receiver location is summed over a large (presently 250) number of sources.
4. The local ENT power in the nearest four $5° \times 5°$ subcells is propagated by the groundwave algorithm and summed at the receiver location.
5. The summed available power at the receiver is converted to the decibel value Fa. Fa is treated as the median of the normal distribution from which the level exceeded a chosen percentage of time is computed.

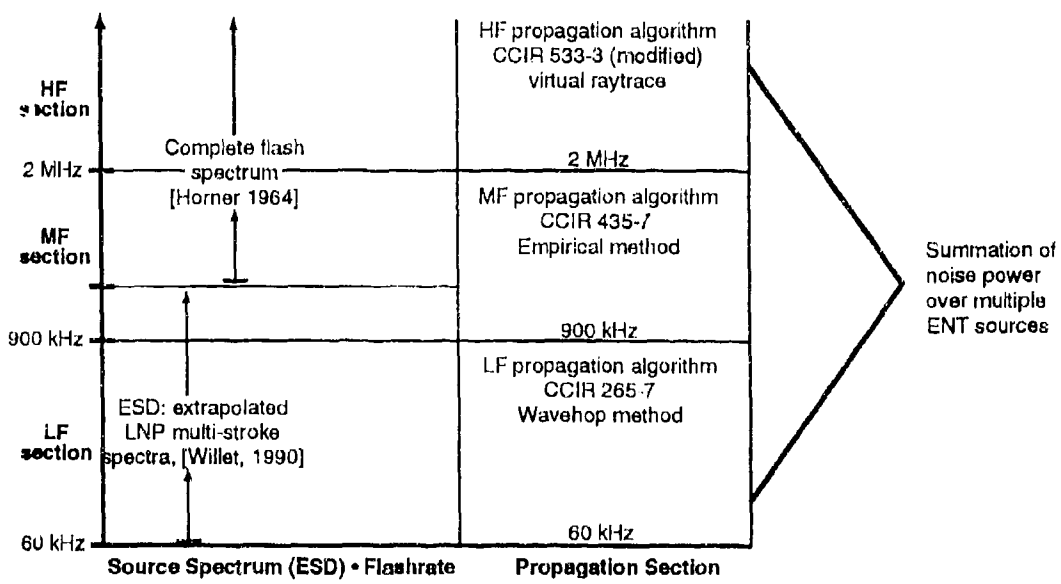

Figure 10-1. Flow chart for NoiseProp computations.

10.2 Discussion

1. The conversion of GLO or DGLO map flashrate data into ENT map power data is a weighted sum of return stroke and bipolar in-cloud stroke spectra for frequencies below 1 MHz. Above 1 MHz a complete flash spectrum is utilized as discussed in Section 4.0. Flash power standard deviations are calculated as in Warber and Field [1991]. This requires weighted sums of stroke power variances. Above 1 MHz we do not use separate stroke phenomenology for the overall flash power. Due to the lack of data on flash power standard deviations (at HF) comparable to that available at VLF (and used in LNP) we have carried over the LNP formalism to compute standard deviations above 1 MHz. The overall flash spectrum (straight line in Figure 4-1) is converted by fractional multipliers into a sum of fictitious stroke spectra (return stroke, horizontal and vertical bipolar in-cloud) for which standard deviation expressions are available. Then the standard deviation can be built up for the overall flash using the existing LNP formalism. The overall flash variances from each ENT are summed together to give a total noise variance. The total variance is used to determine the distribution (assumed log-normal) of the overall noise power and the corresponding exceedence level for a given percentage of time.

2. The preliminary sorting of ENTs into a dominance order is done by comparing P_{ENT}/d^2 where P_{ENT} is the ENT power in watts and d is the distance from the ENT center of mass to the receiver in km. This very roughly orders ENTs according to their propagated strength if they propagated in free space. We found it necessary to add up a large number of sources from this presorted ordering using the actual LF, MF, or HF propagation algorithms. This is because the propagation functions are, in fact, not monotonic with distance, especially at HF where the skip distance phenomenon is pronounced. Originally, we had intended to simply observe the size of the power sum as each propagated ENT was added and to terminate the calculation when the increment in the sum was smaller than some small fraction of 1 dB. However, we found many cases where although the stopping criterion was set, subsequent ENTs in the dominance ordering contributed significant power to the cumulative sum. Therefore, at present, we add the first 250 (out of 648) ENTs in every calculation. Although this number is sufficiently large not to miss any significant ENTs, it is admittedly a serious limitation in the time economy of the NoiseProp program.

3. The skywave and groundwave algorithms in NoiseProp all compute the RMS field strength E in dB (μV/m). Then $e = 10^{E/20\ (dB)}$ is the RMS field strength in the vicinity of the receiving antenna in units of μV/m and the associated power flux is $p = e^2/Z_0$ in watts/m^2

where $Z_o = 120\pi$ is the impedance of free space. The available power at the terminals of the receiving antenna is then

$$P_{avail} = p \bullet A \bullet g \qquad (10.1)$$

where ρ is the power flux, A is the effective isotropic antenna aperture area and g is the receiving antenna gain [Stutzman and Thiele, 1981]. Since $A = \lambda^2/4\pi$ where λ is the wavelength in meters, we have

$$P_{avail} = \frac{e^2}{Z_o} \bullet \frac{\lambda^2}{4\pi} = \left(\frac{\lambda^2}{480\pi^2}\right) \bullet e^2 g = \frac{e^2 \bullet g}{9\times10^8 \bullet 480\pi^2 \bullet f_{MHz}^2} \text{ (watts)}. \qquad (10.2)$$

The gain is nominally set to unity and the numbers p_{avail} are summed over all contributing ENT sources to yield the overall noise power in watts at the receiving antenna terminal. (Note: if we express dB values by using capital letters, the above equation becomes

$$P_{avail} = E + G - 107.2 - 20 \log_{10} f \text{ MHz} \qquad (10.3)$$

which is the commonly used relation seen in all the standard propagation prediction codes.)

11.0 CALIBRATION OF NOISEPROP MODELS

The NoiseProp system consists of two sections; the ENT source algorithm and the propagation algorithms (LF, M, HF, groundwave). The propagation algorithms can be verified to a certain extent by comparison with certain existing well tested propagation codes. In the case of the HF section, extensive comparisons were made for many circuits with the IONCAP [Lloyd et al., 1978] and ASAPS [see Sailors and Rose, 1993] prediction codes. The codes are considered benchmarks because they have been checked and adjusted against real measurements for many years. The LF wave hop code can be tested to a certain extent against the empirical CCIR 435-7 method which works down to 150 kHz.

The largest source of uncertainty, however, is the lack of precise data on lightning flash power spectra above the VLF range. This introduces a systematic error into all results which is a function of frequency and which can be corrected for, a-posteriori.

A-posteriori corrections were introduced by a set of comparisons with the CCIR 322-3 [CCIR, 1988] noise model at the 50th percentile level. The CCIR model was based on noise data taken at 16 stations during the period 1957 through 1966 (not all the stations produced data for the entire period). The data were grouped into four seasonal blocks and six four hour time blocks during each day of the seasonal block. The CCIR model contains median hourly values of RMS noise power in each time block; the median is taken with respect to the seasonal (~90 day) aggregates. The 16 station median values are smoothly interpolated onto a worldwide grid using spherical polynomial expansions [Spaulding and Washburn, 1985]. The coefficients in this expansion are the basis for a computerized version of the maps in CCIR 322-3.

Systematic corrections to the NoiseProp predictions take the form of a function of both frequency and local time (at the receiver site). The frequency dependence offsets errors in the ENT source power spectrum (which will factor systematically through all subsequent stages). The local time correction is to offset any cumulative systematic errors in the propagation algorithms themselves inasmuch as these algorithms all contain strong local time variations in their propagation loss modeling. A local time correction also allows for accounting of non-specific diurnal trends in local lightning activity not explicitly included in the stroke and flash rate models.

The correction terms were computed by averaging the dB difference between CCIR 322-3 and NoiseProp over four month ensembles of 12 CCIR station measurements in 4-hour blocks. The station sites ae shown in Figure 11-1. The output of the CCIR 322-3 model is assumed to be closest to the underlying data at the data collection locations themselves and at greater variance with reality in areas far from the 16 station measurement network, e.g., over oceans [Sailors, 1993]. The four months were January, April, July, and October; hence, seasonal effects are averaged out. Since the averages were over 12 widely separated locations; station specific effects are also averaged out. These ensemble averages were computed at 100, 500, 1000, and 1500 kHz to calibrate the LF and MF sections; 5, 10, 15, and 20 MHz to calibrate the HF section. The resulting calibration curves are smoothly approximated by least-squares polynomials in local time and linearly interpolated as functions of frequency. That is, we compute

$$\Delta(\text{local time, f kHz}) = \underset{\substack{\text{12 stations} \\ \text{4 months}}}{\langle \text{NoiseProp - CCIR} \rangle} \text{ (dB)} \quad . \qquad (11.1)$$

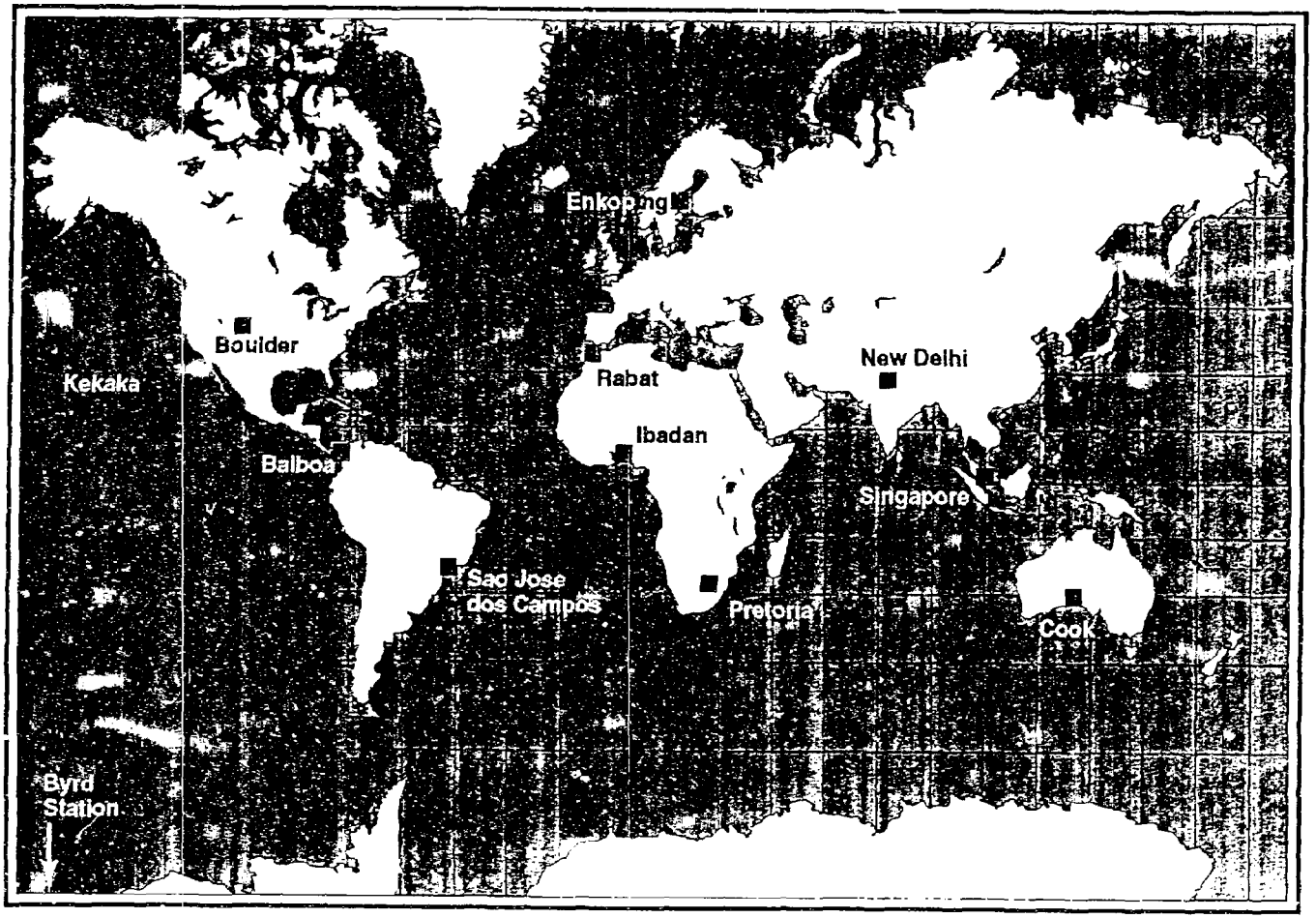

Figure 11-1. CCIR station sites used in NoiseProp calibration.

These calibration curves are shown for the eight base frequencies in Figures 11-2 and 11-3.

The correction term Δ is then subtracted from the uncalibrated NoiseProp output after each propagation calculation. Examples of NoiseProp output after calibration are shown in Figures 11-4 and 11-5. Figure 11-4 is a set of LM-HF noise calculations for July, 0000 UT and low

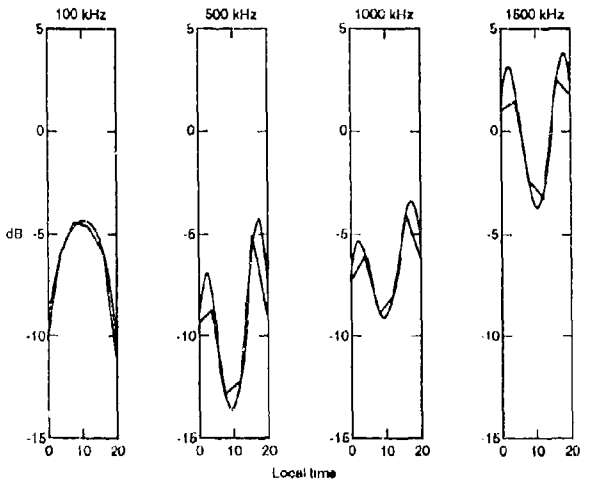

Figure 11-2. LF-MF NoiseProp calibration curves at 100, 500, 1000, and 1500 kHz. A smooth polynomial fit is superimposed upon the actual data. These curves are subtracted from the NoiseProp output to account for systematic frequency dependent and local-time dependent deviations. The curves are linearly interpolated in frequency.

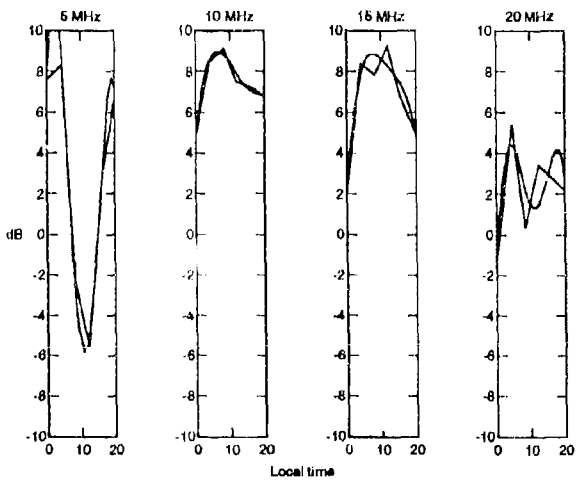

Figure 11-3. HF NoiseProp calibration curves at 5, 10, 15, and 20 MHz.

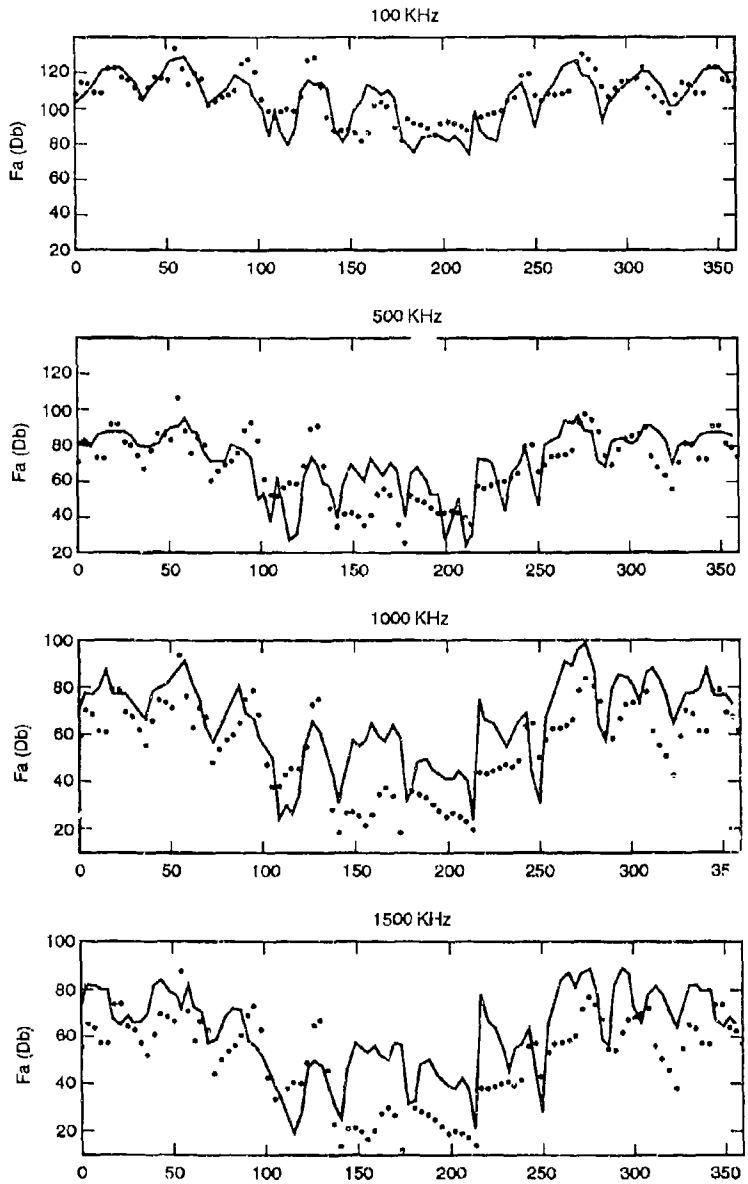

Figure 11-4. Typical LF-MF NoiseProp output (after calibration). Values are in dB with respect to kTb, at the 50-th percentile (median). See text for explanation of x-axis. July, 0000 UT, low solar activity.

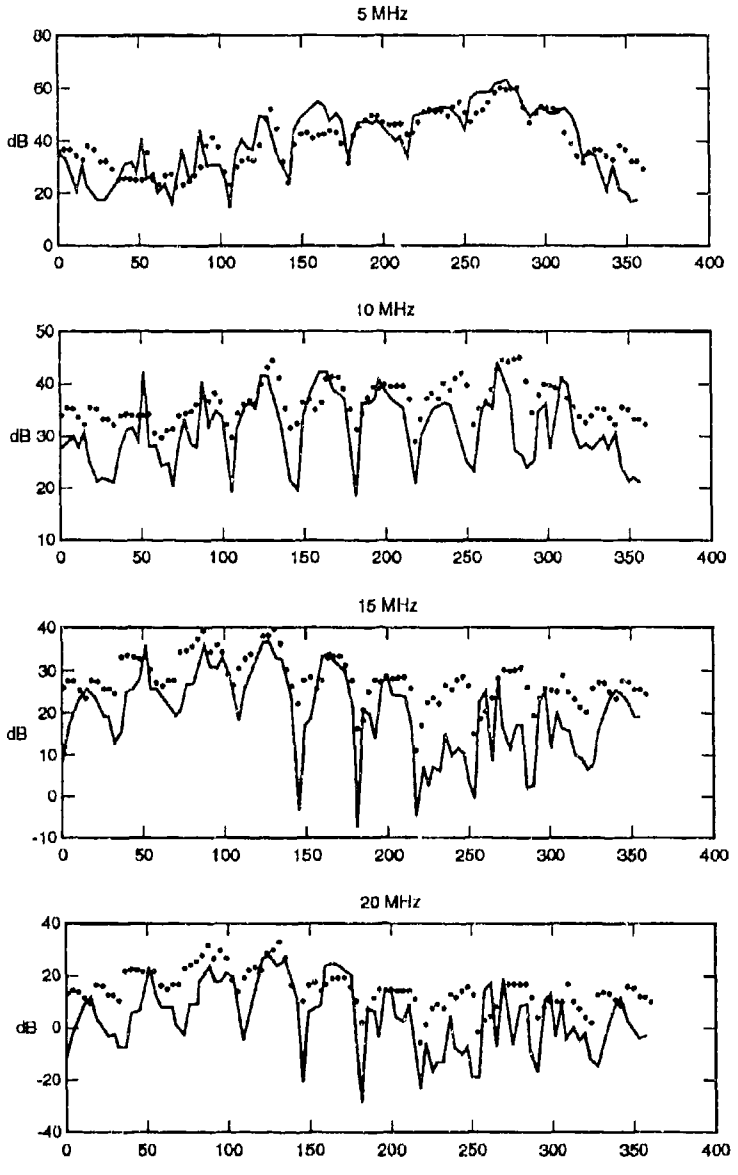

Figure 11-5. Typical HF NoiseProp output (after calibration). July, 0800 UT, low solar activity, low geomagnetic activity index. See text for explanation of x-axis.

sunspot activity. The solid curves are the NoiseProp calibrated values; the dots shown CCIR values. Figure 11-5 is a typical set for HF at about 0800 UT. The graphs show the result of 100 calculations at 10 longitudes from 0 to 360°; at each longitude calculations were done at 10 latitudes between -60 and 60°; this sequence of calculations is plotted in natural ordering of

$$\left\{\left\{(\mathrm{lon}_i, \mathrm{lat}_j)\right\}_{j=1,10}\right\}_{i=1,10} \text{ given by } K = 1,2,3,\ldots, 100 \quad \text{where} \quad K = 10 \bullet (i-1) + j.$$

The pattern of minima at the extremes of latitude (±60°) and maxima at the equator is seen in both the NoiseProp and CCIR models. The minima in the CCIR plots are not as deep as the NoiseProp minima. This may reflect the fact that the CCIR model is constrained so as to smoothly fit a sparse set of data (16 points) to the worldwide grid. Far from data points, the properties of the fit are largely determined by the nature of the fitting expansion, which is smooth and slowly varying rather than by the underlying physical phenomena being approximated [Sailors, 1993].

Ideally, testing of a source based noise model such as LNP or NoiseProp should be done with source distributions representing the actual distribution of lightning sources during the period of a noise measurement. Clearly this cannot be applied to the CCIR 322-3 model which represents long term median noise levels measured over a great variety of (many years) meteorological conditions. Nor is it at all completely obvious that the median noise measurements are necessarily congruent to a NoiseProp prediction utilizing *median* (long term) GLO maps. The nonlinearity in the propagation mechanism will alter the probability distribution of ENT intensities when it is transformed to a probability distribution of noise power summed over many sources. The best program for validation and calibration requires an active field measurement program simultaneous with the processing of current meteorological data into dynamic DGLO maps which are input to NoiseProp (and LNP).

12.0 NOISEPROP APPLICATIONS USING DYNAMIC LIGHTNING OCCURRENCE MAPS

This section describes the development of an operational dynamic lightning forecasting system. Such a system will produce the DGLO maps from meteorological data which can serve as input data to the LNP or NoiseProp noise prediction codes. The replacement of the long term median GLO maps (derived from satellite observations) with dynamic DGLO maps will be transparent

for the operation of the NoiseProp code; the GLO and DGLO map files will have identical data formats. The DGLO maps will contain DGLO forecast based data in those sectors where adequate meteorological data is available; they will contain the original GLO data in sectors where forecasts could not be made (due to insufficient data at a given time and place).

We have developed several techniques for converting short, medium, and long term weather forecasts (along with other parameters) to produce lightning flash rates. These predictions will be assembled into the DGLO maps and be made available to users by downloading from a central location. Only the military produces weather forecasts on a worldwide basis. It appears that access to data from the Air Force Global Weather Central (AFGWC), in particular, will be needed on a regular basis for high confidence forecasts. A detailed feasibility study for the lightning forecasting problem is given in a companion report by Warber and Sinclair [1995].

12.1 Correlation Between Flash Rate and Weather Parameters

In this section we summarize the relationships we have found between lightning flash rates and certain weather parameters. The details of the derivations can be found in Warber and Sinclair [1995].

To be useful, these weather parameters must be available globally and forecast up to several days into the future; or else they must be derivable from such parameters. For the correlation study, two primary data sets were used: a lightning flash rate archive and a cloud phenomenology archive. Archived lightning flash rate data is available from the National Lightning Detection Network (NLDN), a system of 100 sensors that record the position, time, number of return strokes, and other parameters for cloud-to-ground flashes in the U.S.. The sensor sites are shown in Figure 12-1. The NLDN data has a nominal spatial resolution of 10 km [Orville, 1990]. Figure 12-2 shows lightning flashes detected by the NLDN in four UT time blocks. Cloud top height and thickness (optical depth) and two other parameters were derived from the International Satellite Cloud Climatology Project (ISCCP) archive. The ISCCP data includes over 132 parameters grouped by 3-hour time blocks and a nominal 250 km spatial resolution. The correlation study utilized data from both NLDN and ISCCP for the period July 1990. In addition to the ISCCP data, a set of National Weather Service radar summary maps for July 1990 and a set of weather forecast maps for that period were used [Warber and Sinclair, 1995].

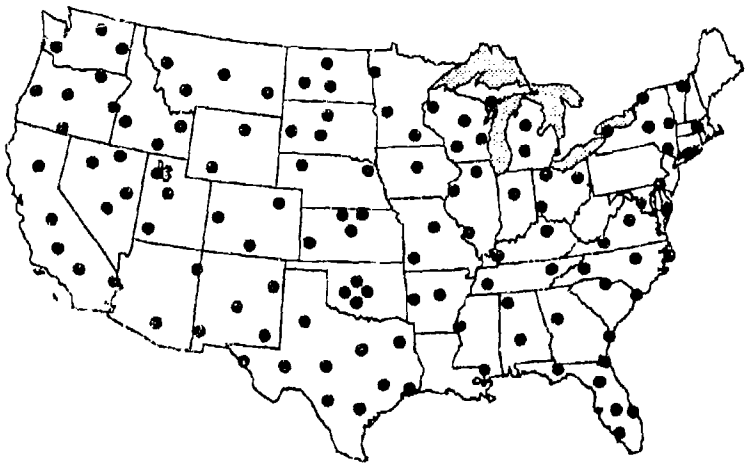

Figure 12-1. Location of over 100 magnetic direction finders in the National Lightning Detection Network (NLDN).

Correlations were sought between lightning flash rates and the following four quantities derivable from the ISCCP observables:

1. Convective cloud top height, Z_{cct}
2. All cloud top height, Z_{ct}
3. Lifted index, L_I
4. Convectively Available Potential Energy (CAPE).

In addition, correlation between flash rates and a heuristically weighted thunderstorm density derived by analysis of weather maps was studied. The four parameters above are all derivable by standard equations from the basic observables recorded in the ISCCP. In particular, convective cloud top height can be inferred by discriminating deep convective clouds from others using the ISCCP cloud optical depth data in combination with ISCCP cloud top pressure data. Cloud top heights are computed from cloud top pressures by the standard calculation for the altitude at which an ideal gas in a uniform gravitational field reaches a given pressure, under the assumption that the rate of temperature decrease between pressure levels is constant. The ISCC data set also contains the information needed to calculate the lifted index (L_I) and CAPE, both of which are related to the virtual temperature versus altitude profile of an air mass (see Warber and Sinclair [1995] for detailed derivations).

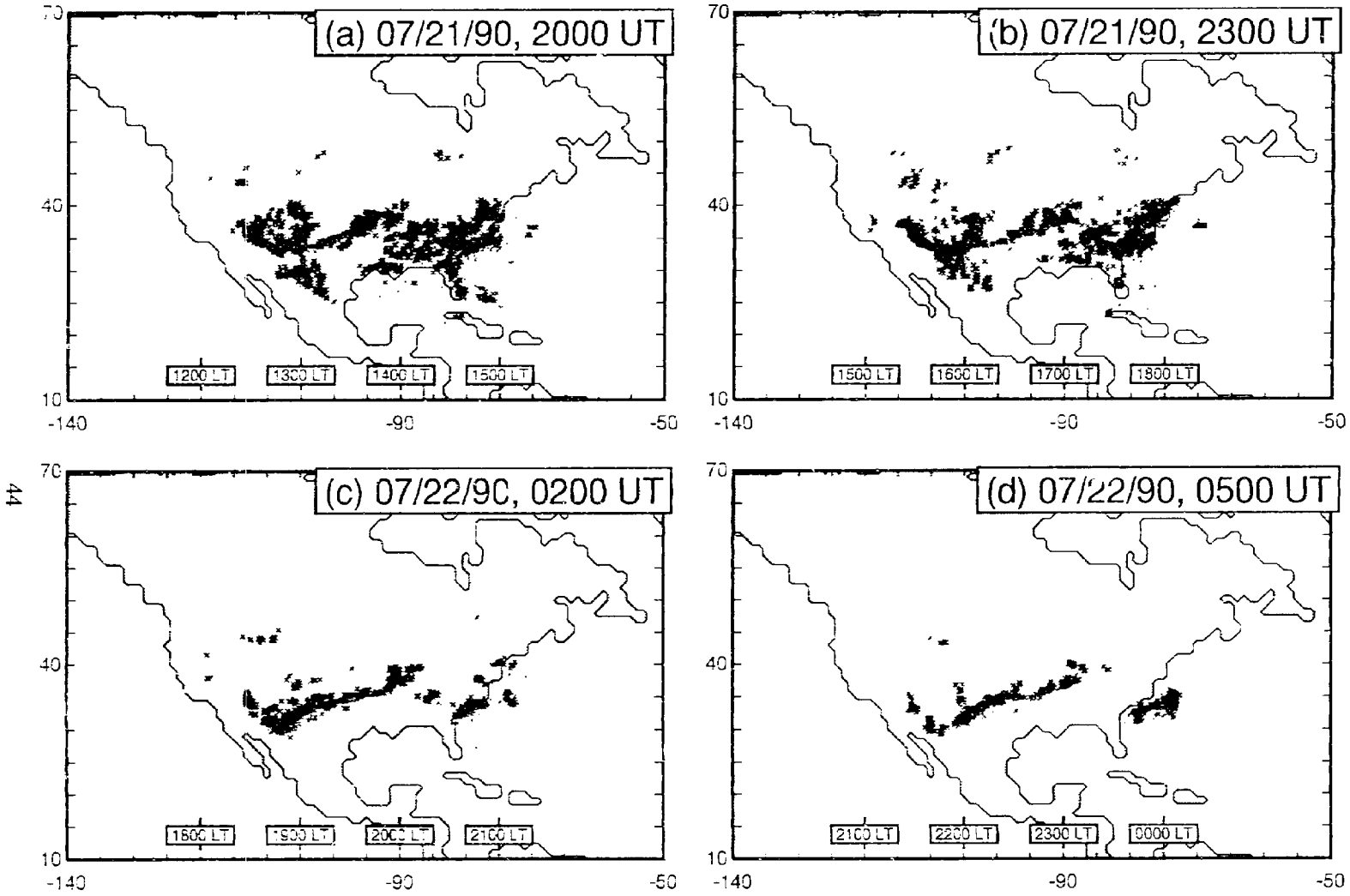

Figure 12-2. Lightning flash locations for 21-22 July 1990 measured by the NLDN. Each mark shows the location of a flash that occurred within one hour after the time shown on the figure. The local time is shown along the bottom of each figure.

The correlation analysis proceeds by first determining a least-squares fit between flash rate and the chosen climatological parameter from 1 through 4 above. All the relationships could be fit as least-squares lines on log-log or log-linear graphs. The fit for CAPE is shown in Figure 12-3. Data from the first 15 days of July 1990 were used to determine the fits. Data points with observed flash rates of zero were not used. After a fit was found, data from the second 15 days of the month were used to check the stability of the fit. During the check all data points, both zero and non-zero observed flash rates were used. This was to check whether the fit, which is determined from only non-zero flash rates, predicts lightning flashes when, in fact, there are none. Two correlation coefficients were then computed: that between the first 15 days of flash rate data and the fit (based on that data) and that between the second 15 days of data and the predicted values (using the fit derived from the first 15 days). If both correlation coefficients are greater than 0.5 (in magnitude) we conclude that the fit is a stable and consistent predictor of flash rate from the given weather parameter. In instances where the check correlation falls below 0.5, however, we conclude that either 1) the slope of the relation between flash rate and the chosen weather parameter changes significantly over the course of a month, or 2) the predictor gives significant flash rates where, in fact, there are none.

In particular, the lifted index and all cloud top height, L_I and Z_{ct} were found to be inadequate predictors of flash rate when taken by themselves (in the absence of other information). The following conditions, when satisfied, combined L_I or Z_{ct}-based predictions raise the check correlations into the significance range (0.65 to 0.75):

1) If there is a thunderstorm predicted for any $2.5^\circ \times 2.5^\circ$ subsquare.
2) If the subsquare had lightning in it during the previous 24 hours.
3) If the subsquare is over a mountainous region and cloud top pressure is less than 300 mb (use with L_I predictions)
4) If the subsquare is in the path of an ongoing storm system (requires radar storm summary maps).

These four auxiliary conditions, when used to select restricted subsets of weather data for lightning flash rate predictions will be referred to as *predictors* or *auxiliary predictors*.

The fits between flash rate and the four weather parameters above, Z_{cct}, Z_{ct}, L_I, and CAPE were:

1) Convective cloud top height: $F = 2.93 \times 10^{-7}\ Z_{cct}^{4.7}$ sec^{-1} sq^{-1} (1 sq $\equiv 5^\circ \times 5^\circ$ area).

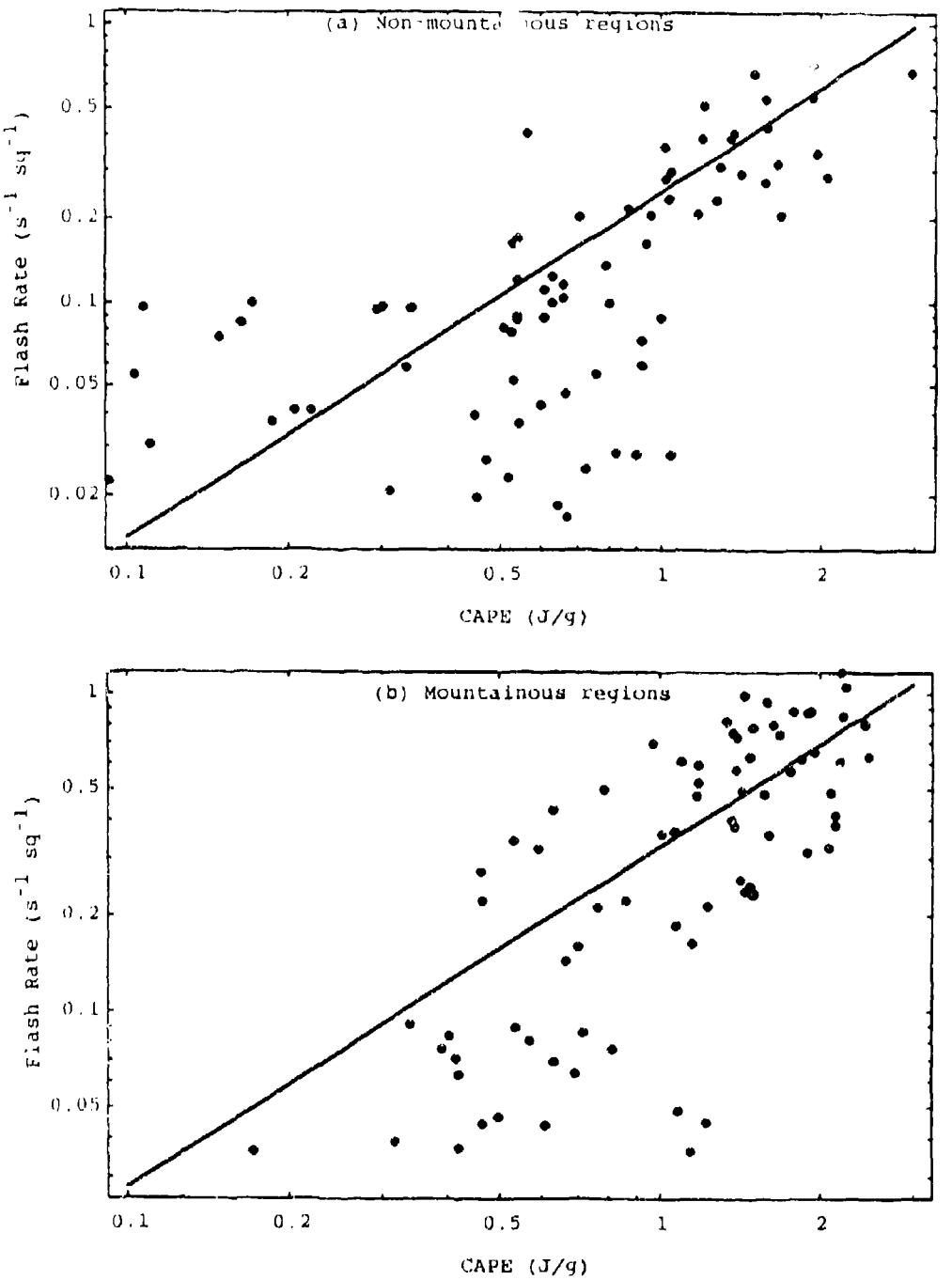

Figure 12-3. The fit found between flash rate and convectively available potential energy (CAPE), solid line, and examples of observed data from the NLDN for (a) non-mountainous and (b) mountainous regions.

2) All cloud top height (must use one auxiliary predictor): $F = 3.73 \times 10^{-7} Z_{ct}^{4.7}$ sec^{-1} sq^{-1}

3) Lifted Index (must use one auxiliary predictor):

$F_{NM} = 4.8 \times 10^{-2} \exp(-0.42\ L_I)$ sec^{-1} sq^{-1} (non-mountain region)

$F_M = 2.7 \times 10^{-2} \exp(-0.47\ L_I)$ sec^{-1} sq^{-1} (mountain region)

4) CAPE:

$F_{NM} = 0.25\ CAPE^{1.25}$ sec^{-1} sq^{-1} (non-mountain regions)

$F_M = 0.33\ CAPE^{1.07}$ sec^{-1} sq^{-1} (mountain regions).

A fifth prediction method derives flash rates directly from the extent of area covered by severe weather. A few days worth of weather maps from July 1990 were digitized and overlaid with a $2.5^\circ \times 2.5^\circ$ grid. Each subsquare containing a thunderstorm prediction was marked and assigned the value 1. Then each marked subsquare that had marked subsquares on all four sides was assigned the value 2. Then each subsquare with a value 2 that had adjacent subsquares with the value 2 was given the value 3. The process was repeated until no subsquares were changed. Then the subsquares were assigned the following flash rates:

- $F_{NM} = 0.2 \times \text{value}^{1.1} \bullet n(h)$ sec^{-1} sq^{-1} (non-mountain)
- $F_M = 0.1 \times \text{value}^{1.2} \bullet n(h)$ sec^{-1} sq^{-1} (mountain)

where the values 1.1 and 1.2 were found to give the best fit to observed flash rates and n(h) is the normalized local time dependence factor for the local time of day or the prediction. Figure 12-4 shows the factor n(h). (This diurnal curve was derived by grouping all the July 1990 NLDN flash rate data in local time blocks.) The overall correlation between observation and prediction was lower than that using the other methods. In the absence of other data, however, these weather map fits can be used to make rough predictions.

In the following we discuss the lightning forecasting methods we have developed with a view toward applications. We have divided the lightning forecasts into three categories: short, mid, and long term forecasts. Short-term forecasts are those made up to 12 to 18 hours in advance, mid-term forecasts are made 24 to 48 hours in advance, and long-term forecasts are made for periods beyond 48 hours. These types of forecasts are distinguished by the methods used to make them and the confidence we have in the results.

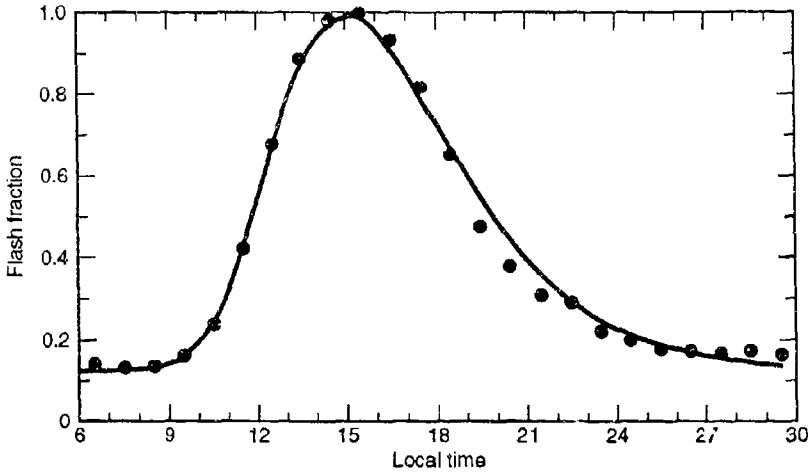

Figure 12-4. Number of lighting flashes per hour as a function of local time in July, 1990 over all NLDN sensors. Normalized to 1 at 1530 LT.

12.2 Short-Term Forecasts

We use data sources in order of reliability: a) direct lightning measurement systems, e.g., NLDN, b) cloud top heights directly from weather radar, and c) cloud top heights inferred from satellite images. Using a, b, or c we determine the current lightning distribution (by the fits for cloud top height and an auxiliary predictor for b, c). The flash rate is determined for each 2.5° × 2.5° subsquare. This initial distribution is called the flash rate basis. Subsquares in the basis are then grouped into storms. The storm track is then projected up to 24 hours ahead (using the current lightning distributions and distributions from the past to determine how the center of each storm is moving). The basis flash rates are copied to the subsquares around the new storm center. The new flash rate basis is adjusted using the diurnal curve in Figure 12-4. If we write the basis flash rate as F_o and the basis local time at a subsquare as to then the adjusted value is:

$$F_p = F_o \bullet n(t_p)/n(t_o)$$

where the local time for the forecast is t_p.

12.3 Mid-Term Forecasts

Mid-term forecasts will be based either on predicted CAPE or predicted L_J and one auxiliary predictor. The NWS predicts lifted index every 12 hours for he periods 12, 36, and 48 hours into the future.

12.4 Long-Term Forecasts

Long-term forecasts will be based on the weather map correlation (fifth prediction procedure above). This requires that 48 hour severe weather predictions are available regularly. For noise forecasts based on long term forecasted flash rates it is more reliable to give ranges, e.g., 2 dB above or below the normal average, 2 to 5 dB, 5 to 8 dB, 8 to 11 dB, 11 to 15 dB, or 15 dB above or below the normal average noise level (determined from the original GLO maps).

12.5 Conclusions and Recommendations

In this section we have described the techniques needed to create an operational dynamic noise prediction system. The NoiseProp noise model will accept DGLO data produced by the prediction methods discussed above to generate DGLO files which are transparent to the NoiseProp computer code. The DGLO prediction codes will need regular access to data from external sources. The Navy's Fleet Numerical Meteorology and Oceanographic Center (FNMOC) and the AFGWC generate the kind of data we need for flash rate predictions on a global scale. AFGWC has expressed interest in providing forecast data which would be needed in the lightning prediction codes. It seems that the best way to implement such a system will be for a central location to collect the needed weather data and process it into the DGLO maps. These maps would then be made available for downloading. A computer system will have to be created to completely automate the forecasting method which is presently far too labor intensive to operate on a daily basis. The forecast algorithms must also be updated over time as larger numbers of predictions and measurements are correlated. In this last regard, the forecasting system would have to undergo a training period. The present report's prediction fits are provisional insofar as they are derived from one month of data on one continent only.

13.0 REFERENCES

Abramowitz, M. and I. A. Stegun, *Handbook of Mathematical Functions*, National Bureau of Standards, US Government Printing Office, Washington, DC, 1972.

Barghausen, A. F. et al., *Predicting Long Term Operational Parameters of High-Frequency Sky-Wave Telecommunications Systems*, ESSA Technical Report ERL 110-ITS 78, U.S. Department of Commerce, Boulder, CO, 1969.

Bilitza, D. et al., *International Reference Ionosphere 1990*, NSSDC/WDC-A-R&S 90-22, National Space Science Data Center/World Data Center A for Rockets and Satellites, Greenbelt, MD, November 1990.

Bremmer, H. *Terrestrial Radio Waves*, Elsevier, Netherlands, 1949.

Budden, K. B., *Radiowaves in the Ionosphere*, Cambridge University Press, Cambridge, UK, 1966.

-----, *The Wave-Guide Mode Theory of Wave Propagation*, LOGOS Press, London, 1961.

Cambridge Computation Laboratory, *Tables of the Modified Hankel Functions of Order One-Third and of Their Derivatives*, Harvard University Press, Cambridge, MA, 1945.

CCIR (International Radio Consultative Committee), Report 340-1, International Telecommunications Union, Geneva, Switzerland, 1966.

-----, Report 340-2, International Telecommunications Union, Geneva, Switzerland, 1967.

-----. *Interim Method for Estimating Sky Wave Field Strength and Transmission Loss at Frequencies Between 2 and 30 MHz*, Report 252-2, International Telecommunications Union, Geneva, Switzerland, 1986.

-----, *World Distribution and Characteristics of Atmospheric Radio Noise*, Report 322-3, International Telecommunications Union, Geneva, Switzerland, 1988.

-----, *Sky-Wave Propagation and Circuit Performance at Frequencies Between About 30 kHz and 500 kHz*, Report 265-7, International Telecommunications Union, Geneva, Switzerland, 1990.

-----, *CCIR Reference Ionospheric Characteristics and Methods of Basic MUF, Operational MUF, and Ray-Path Prediction*, Recommendation 434-5, International Telecommunications Union, Geneva, Switzerland, 1992a.

-----, *Sky-Wave Field Strength Prediction Method for the Broadcasting Service in the Frequency Range 150 to 1600 kHz*, Recommendation 435-7, International Telecommunications Union, Geneva, Switzerland, 1992b.

-----, *CCIR HF Propagation Method*, Recommendation 533-3, International Telecommunications Union, Geneva, Switzerland, 1992c.

Central Radio Propagation Laboratory (CRPL), *Ionospheric Radio Propagation*, National Bureau of Standards Circular 462, U.S. Department of Commerce, Washington, DC, June 1948.

Davies, K., *Ionospheric Radio*, Peter Peregrinus Ltd., London, United Kingdom, 1990.

Davis, P. M., Jr., *Short-Term Prediction of F2-Layer Maximum Usable Frequencies from Local Magnetic Activity*, Technical Report ERL 157-175-100, Institute for Telecommunication Sciences, Boulder, CO, 1970.

Fricker, R., "A Microcomputer program for HF Field Strength Prediction," *Fifth International Conference on Antennas and Propagation*, Part 2, *Propagation, Institute of Electrical Engineers*, IEE, United Kingdom, 1987.

Greifinger, C., et al., *Modeling of TM and TE VLF Atmospheric Noise*, Research and Development Associates, RDA-TR-0226128902-001, August 1989.

Hatfield, V . E. and G. Smith, *AMBCOM User's Guide for Engineers*, Air Force Contract F0 8606-85-C-0018, SRI International, Menlo Park, CA, January 1987.

Horner, F., "Radio Noise From Thunderstorms," in J.A. Saxton (Ed.), *Advances in Radio Research*, Vol. 2, Academic Press, New York, 1964, pp. 121-204.

Hortenbach, K. J., and F. Rogler, "On the Propagation of Short Waves Over Very Long Distances: Predictions and Observations," *Telecommunications Journal*, 46, pp. 320-327, 1979.

Inuki, H., et al., "Development of the Computer Program for Predicting LF and MF Sky-Wave Field Strengths," *Radio Research Journal*, Vol. 29, No. 152, September 1983, pp. 467-485, (in Japanese)

Johler, J. R., "Propagation of the Low-Frequency Radio Signal," *Proceedings of the IRE*, April, 1962, pp. 404-427.

-----, "On the Analysis of LF Ionospheric Radio Propagation Phenomena," *Journal of Research of the National Bureau of Standards-D. Radio Propagation*, Vol. 65D, No. 5, September-October 1961.

Kotaki, M., "Global distribution of atmospheric radio noise derived from thunderstorm activity," *Journal of Atmospheric and Terrestrial Physics*, Vol. 46, No. 10, 1984, pp. 867-877.

Kotaki, M., and C. Katoh, "Global Distribution of Atmospheric Radio Noise Derived from Distribution of Lightning Activity," *Journal of Radio Research Laboratory* (Tokyo), Vol. 30, No. 129, 1983.

LeVine, D. M., "Review of Measurements of the RF Spectrum of Radiation from Lightning," *Meteorology and Atmospheric Physics*, Vol. 37, 1987, pp. 195-204.

Lloyd, J. S. et al., *Estimating the Performance of Telecommunications Systems Using the Ionospheric Transmission Channel*, National Telecommunications and Information Administration (NTIA), Boulder, CO, 1978.

Maxwell, E. L. et al., *Development of a VLF Atmospheric Noise Prediction Model*, Westinghouse Georesearch Laboratory, Boulder, CO, Report 70-1H2-VLF NO-R1, 30 June 1970.

Nanevicz, J. E. et al., "Observation of Lightning in the Frequency and Time Domains," *Electromagnetics*, Vol. 7, 1987, pp. 267-286.

Orville, R. E., "Lightning Ground Flash Density in the Contiguous United States -- 1989," *Monthly Weather Review*, Vol. 119, No. 2, 1991, pp. 573-577.

PoKempner, M., *Comparison of Available Methods for Predicting Medium Frequency Sky-Wave Field Strengths*, NTIS Report 80-42, National Telecommunications and Information Administration, Boulder, CO, 1980.

Sailors, D. B. and R. B. Rose, *HF Sky-Wave Field Strength Predictions*, Technical Report 1624, Naval Command, Control and Ocean Surveillance Center, RDT&E Division, San Diego, CA, September 1993.

Sailors, D., *A Discrepancy in CCIR Report 322-3, Radio Noise Model: The Probable Cause and a Recommended Solution*, Technical Report 2496, Naval Command, Control and Ocean Surveillance Center, RDT&E Division, San Diego, CA, 1993.

Spaulding, A. D. and J. S. Washburn, *Atmospheric Radio Noise: Worldwide Levels and Other Characteristics*, NTIA Report 85-173, US Department of Commerce, Washington, DC. 1985.

Stuztman, W. L. and G. A. Thiele, *Antenna Theory and Design*, John Wiley, New York, 1987.

Uman, M. A., *The Lightning Discharge*, Academic Press, Inc., Orlando, FL, 1987.

Wait, J. R. and A. M. Conda, "Pattern of an Antenna on a Curved Lossy Surface", *IRE Transactions on Antennas and Propagation*, AP-6, 1958, pp. 348-360.

Wait, J. R., "Diffractive Corrections to the Geometrical Optics of Low Frequency Propagation," in Desirant, M. and J. L. Michiels (Eds.) *Electromagnetic Wave Propagation*, Academic Press, New York, 1960, pp. 87-101.

-----, *Electromagnetic Waves in Stratified Media*, Pergamon Press, New York, 1970.

-----, "Recent Analytical Investigations of Electromagnetic Ground Wave Propagation Over Inhomogeneous Earth Models," *Proceedings of the IEEE*, Vol. 62, No. 8, August 1974.

Warber, C. R. and E. C. Field, Jr., "A Long Wave Transverse Electric-Transverse Magnetic Noise Prediction Model," *Radio Science*, Vol. 30, No. 3, May-June 1995, pp. 783-797.

-----, *Long Wave Noise Prediction*, Vol. 1, *Physical Basis of the Model*, Technical Report DNA-TR-90-224-V1, Defense Nuclear Agency, Alexandria, VA, September 1991.

Warber, C. R. and R. F. Sinclair, *Feasibility of Dynamic Longwave Noise Forecasting*, Report 2605, Pacific-Sierra Research Corporation, Santa Monica, CA, October 1995.

Weidman, C. D. and E. P. Krider, The Amplitude Spectra of Lightning Radiation Fields in the Interval from 1 to 20 MHz," *Radio Science*, Vol. 21, No. 6, November-December 1986, pp. 964-970.

-----, "Lightning Amplitude Spectra in the Interval from 100 kHz to 20 MHz," *Geophysical Research Letters*, Vol. 8, No. 8, August 1981, pp. 931-934.

Willet, J. C., et al., "Lightning Electromagnetic Radiation Field Spectra in the Interval from 0.2 to 20 MHz," *Journal of Geophysical Research*, Vol. 95, No. D12, , November 1990, pp. 20,367-20,387.

Wrenn, G. L. and A. 3. Rodger, "Geomagnetic Modification of the Mid-Latitude Ionosphere: Toward a Strategy for the Improved Forecasting of foF2," *Radio Science*, Vol. 24, No. 1, January-February 1989, pp. 99-111.

Appendix
THE CARE AND FEEDING OF NOISEPROP

1. *System requirements*

NoiseProp requires Windows 95, and approximately 5 MB of disk space.

2. *Installation*

To install NoiseProp, insert disk #1 in the drive. From the **Start** button, select **Run a:\setup**. The installation program will create a Start Menu group and program icon.

3. *Running the program.*

From the **Start** button, select **Programs | NoiseProp | NoiseProp**.

For each run, a time, month, frequency, location, bandwidth, sunspot number, and exceedence are required. An optional K-index can be entered, and multiple frequencies and locations can entered.

Most parameters are entered from the main window. Frequencies and locations are entered from their own windows, accessed through the **Edit** buttons in the main window. To add a frequency or location, enter the desired value and click the **Add** button. To delete a value, double-click the value in the list-box, and click the **Delete** button. To modify a value, double-click the value in the list-box, enter a new value and click the **Replace** button. To finish selecting frequencies and/or locations, click the **OK** button. NOTE: You must click the **Add** button to add values to the list. Just hitting the **Enter** key will close the window without adding the value to the list.

After selecting the desired parameters for a run, click the **Run** button. The generated results are contained in the file **RESULTS.OUT**. The order of values in the file is: Frequency, Time, Longitude, Latitude, F_a(Antenna Noise Figure), F_a (CCIR prediction). Units for F_a are dB above kT_0b, where k is Boltzmann's constant, T_0 is reference temperature (288 K), and b is receiver bandwidth (Hz).

To save or restore parameters, click the **Save** or **Load** button, and enter the desired file name.